Hamburg University of Technology

Bachelor Thesis

The measurement of the Young's modulus of ice with ultrasonic waves

Kulbir Singh Randhawa (Matriculation Number: 21379237)

Hamburg, 15th January 2018

First Examiner: Prof. DSc. (Tech.) Sören Ehlers

Second Examiner: D.Sc. (Tech.) Rüdiger U. Franz von Bock und Polach

Institute for Ship Structural Design
and Analysis (M-10)

Statement of Authorship

I certify that this bachelor thesis has been composed by myself, and describes my own work, unless otherwise acknowledged in the text. All references and verbatim extracts have been quoted, and all sources of information have been specifically acknowledged. It has not been accepted in any previous application for a degree.

_____ _____

(Location, Date) (Signature)

Acknowledgement

First and foremost, praises and thanks to Sri Guru Granth Sahib Ji, for His endless showers of blessings throughout my studies and His indispensable Glance of Grace to complete the research successfully.

I would like to express my sincere gratitude to my supervisors Prof. DSc. (Tech.) Sören Ehlers and D.Sc. (Tech.) Rüdiger U. Franz von Bock und Polach for their expert guidance, ever valuable comments and remarks during this entire bachelor thesis.

Special thanks to Prof. Dr.-Ing. Frank Michael Schmidt-Döhl and Dr.-Ing. Gernod Deckelmann for providing the Krautkrämer USD10 instrument and their invaluable tips during the experiments.

I would like to thank M.Sc. Hauke Herrnring, Andrej Koch and Wittek Ringwelski for their constant help during the manufacturing of the specimens and the construction of the bracket. I am also thankful to the entire employees of the testing hall of the institute for their cooperation and valuable support.

I gratefully acknowledge Nawid Akhondzada for proofreading this bachelor thesis. He pointed out weaknesses, provided necessary suggestions and constructive criticism.

Last but not the least, I wish to thank my father, Jasvir Singh and my mother Paramjit Kaur, and all my family members for their continuous support, motivation, and their wonderful love and patience in completing this thesis

Abstract

Many techniques have been used to measure the Young's modulus of ice. The purpose of this bachelor thesis is to develop a more effective and precise technique. The impulse-echo method has been used to measure the longitudinal ultrasonic velocities of three different types of specimens. From this, the Young's modulus has been calculated. The specimens included homogeneous, inhomogeneous and a cracked polycrystalline ice Ih sample. The homogenous samples studied were found to be elastic isotropic, whereas the inhomogeneous and cracked sample were found to have an anisotropic elastic behaviour. For the cracked specimen, different decreases of the Young's moduli were measured in different directions. The results showed an overall scatter and gives therefore only temporary and rough values for the longitudinal sound velocity in a homogenous polycrystalline ice specimen. Further, the applied method is applicable to detect different types of ice with different composites and manufacturing, and to identify a change of elastic properties after crack.

Keywords: ice, polycrystalline, ultrasonic, sound velocity, mechanical properties, Young's modulus, crack

Contents

List of Figures

List of Tables

List of Equations

List of Symbols

Symbol	Meaning
B	Bulk modulus
b	Breadth-axis
C	Stiffness constant
c	True sound velocity
c_l	Longitudinal wave velocity
c_t	Transversal wave velocity
c_x	Shown velocity of sound
d	True thickness of the specimen
d_x	Indicated thickness of the specimen
E	Young's modulus (modulus of elasticity)
e	Distance of any reflector during the transit-time method
f	Frequency
G	Shear modulus (rigidity modulus)
h	Height-axis
i	integral value
j	integral value
l	Length-axis
m	Mass
S	Compliance constant
T	Temperature
t	Transit time
t_B	Transit time for the back wall echo

T_r	Room temperature
t_R	Transit time for the defect echo
V	Volume
V(T)	Value of any of the fundamental constants depending on the temperature
α	Angle between the direction of loading and the c-axis
ε	Strain
λ	Wavelength
ν	Poisson's ratio
ρ	Density
σ	Applied stress

1 Introduction

In the past decades, the research on ice has grown significantly. Not only for activities, like skiing or skating, also in the science, its new properties are still being explored to the day. Whether to examine the global climate change, to break ice sheets in the arctic with icebreakers, to explore oil in cold oceans, to research the icing conditions in aviation, to delve icy moons or during many other research activities in cold regions, information about the mechanical properties of ice, inter alia, the Young's modulus, are indispensable.

Many experimental techniques in the past were used to determine the Young's modulus of ice. However, they all were complex, very time-consuming and cost-intensive, and partly too imprecise, too. In the ultrasonic technology, several, comparatively simple, keen and time-saving techniques have been explored to measure the mechanical properties of other materials like steel.

In the present work, for the first time, the impulse-echo method is applied and tested on ice samples. Beside a detailed literature research, the focus is on measuring the ultrasonic velocities of different ice specimens, and calculate from this, the Young's modulus of the ice. The target is to review if this technique is applicable to ice samples. If it is, how precise are the results? Is this technique able to replace conventional methods for measuring mechanical properties of ice? Is it possible to measure changes in the elastic properties after an applied force on the specimens?

Therefore, the structural, physical and mechanical properties of ice are analysed first. Afterwards, the principle of ultrasonic testing and the processes are presented and the use of the ultrasonic unit is explained. After the basic knowledge, a state of the art, the practical experiments and its results are described and discussed. At the end of the thesis, a summary of the results, along with a recommendation on further studies, is given.

2 Structure of ice

From the 12 crystalline forms of ice, the stable phase at ordinary pressures is termed ice I (Figure 1). Because the polar ice sheets are too thin, they are not able to reach the critical condition for formation of ice II and ice III. The h represents the hexagonal crystal symmetry, which is reflected in the shape of snowflakes, due to the hexagonal symmetry of the molecular arrangement [Schulson and Duval, 2009; Hobbs, 1974]. Although two other crystallographic structures are known, the cubic structure and the amorphous form, only the hexagonal structure is found in nature [Michel, 1978]. Ice Ih is termed ordinary ice [Schulson and Duval, 2009]. Before any discussion can be made on the influence of ice properties on ultrasonic waves, it is important to analyse the structure of ice Ih.

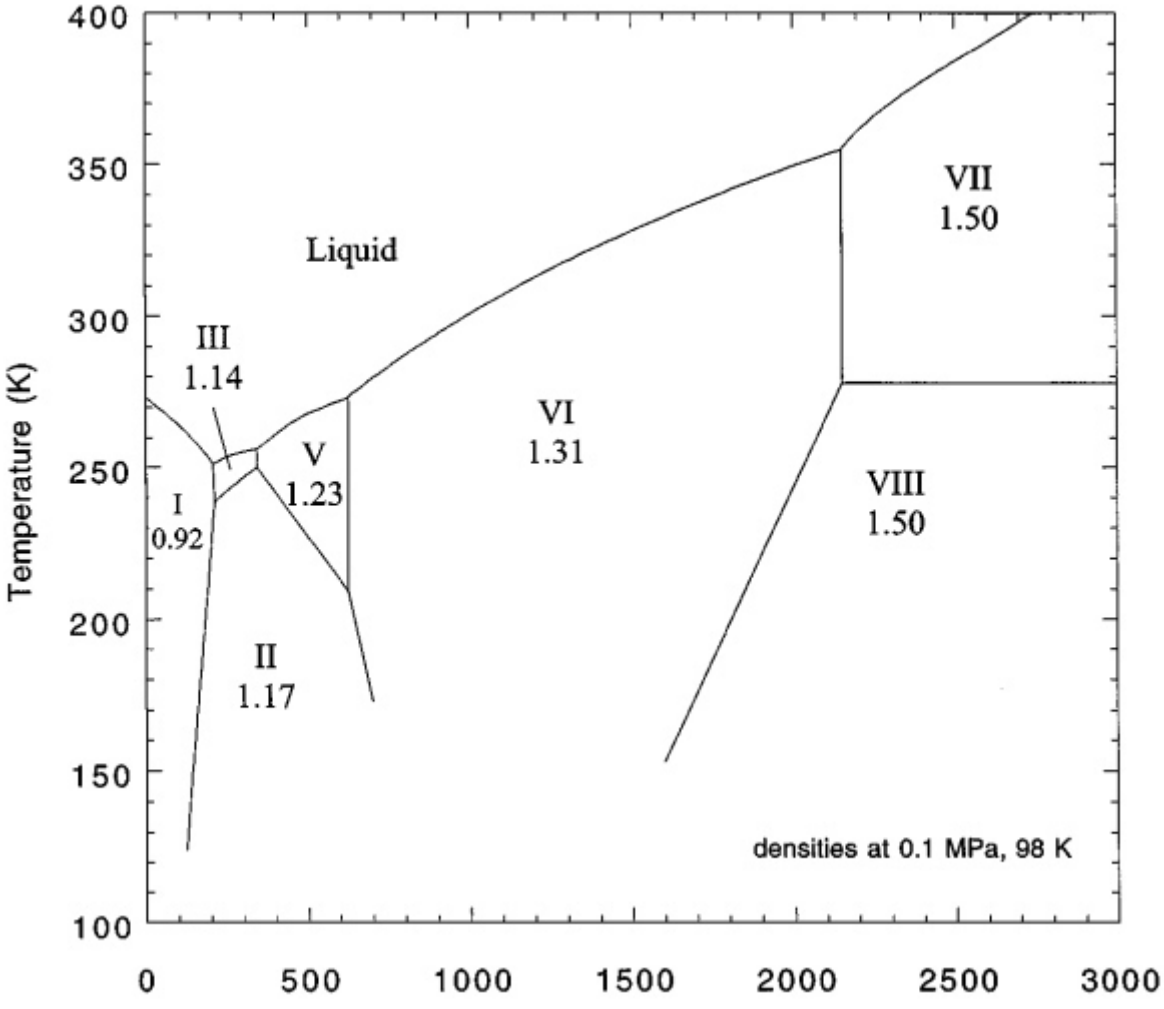

Figure 1: Phase diagram for water ice [Durham and Stern, 2001]

2.1 Crystal structure

Ice Ih has a hexagonal structure. Each oxygen atom in ice Ih must be situated approximately at the centre of gravity of its four neighbouring oxygen atoms. They are arranged in a tetrahedral pattern [Bragg, 1922]. Hexagonal symmetry can be seen by connecting oxygen atoms. The angles between the directions of all oxygen atoms is 109.47°, the O-O distance is 0.276 nm, the O-H distance 0.0985 nm. [Schulson and Duval, 2009].

The arrangement of the oxygen atoms in ice Ih can be seen in Figure 2, the rods joining the oxygen atoms represent bonds, hydrogen atoms are not shown. It shows a number of important features of the molecular structure of ice Ih: The tetrahedral coordination of the oxygen atoms gives rise to a crystal structure possessing hexagonal symmetry. The hexagonal shape exhibited by many ice crystals is clearly related to the hexagonal symmetry of the molecular arrangement. Another important characteristic of the molecular structure is that the molecules are all concentrated close to a series of planes known as the basal planes. The normal to the basal planes is referred to as the c-axis [Hobbs, 1974; Michel, 1978]. Ice Ih does not possess the closely packed crystal structure of the hexagonal metals. Instead its structure is rather open [Schulson and Duval, 2009] and this is reflected in its low density compared to liquid water [Hobbs, 1974; Michel, 1978].

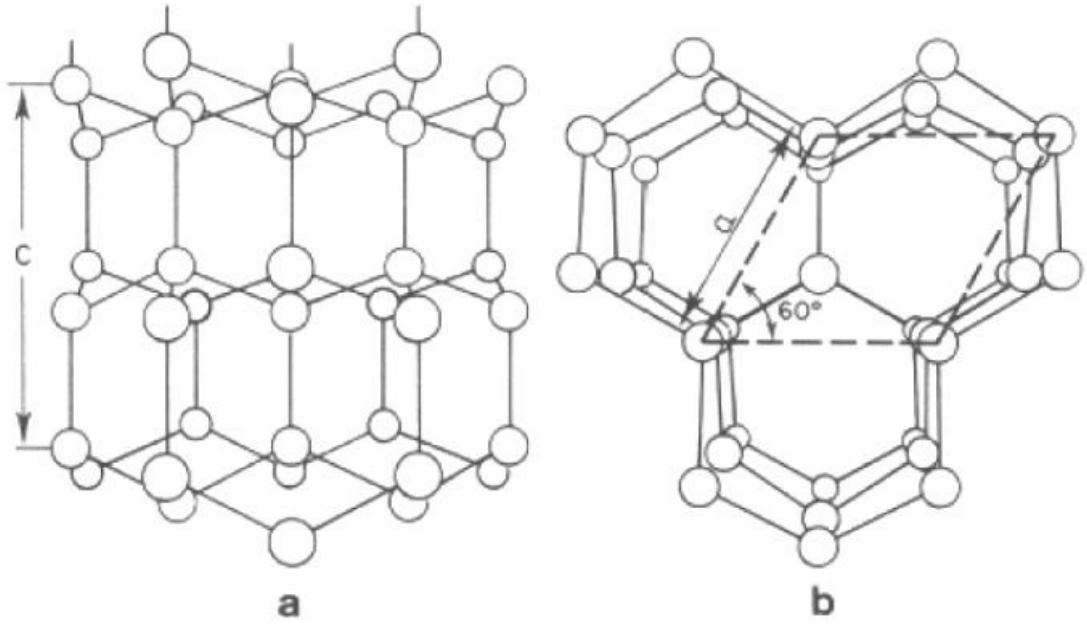

Figure 2: Molecular structure of ice a) perpendicular to the c-axis and b) along the c-axis [Michel, 1978]

It can be seen from Figure 2 that the fundamental building block of the crystallographic structure of ice Ih is the assemblage of oxygen atoms indicated by the parallelepiped drawn in dashed lines in Figure 2. The region of space defined by this group is termed a unit cell. By stacking identical unit cells face to face in perfect alignment in three dimensions, the complete crystallographic structure may be constructed [Hobbs, 1974; Michel, 1978].

In crystallography, the space group $P6_3/mmc$ describes the lattice of oxygen atoms in the Ih structure. The letter P means that the space lattice is primitive. 6_3 means that the principle axis of symmetry, which is the c-axis, is a hexagonal screw axis, that passes through the centre of horizontally oriented, hexagonal puckered ring of atoms [Schulson and Duval, 2009]. The first *m* in the space group symbol indicates that there are mirror planes normal to the principle c-axis of symmetry such that each molecule situated below a mirror plane has a corresponding molecule in a mirror image position above the plane (Figure 3 a)). The remaining two symbols indicate that there are two sets of symmetry planes parallel to the c-axis. A set of mirror planes indicated by the second *m* and a set of glide planes indicated by the *c* (Figure 3 b); Figure 3 c)) [Hobbs, 1974; Michel, 1978].

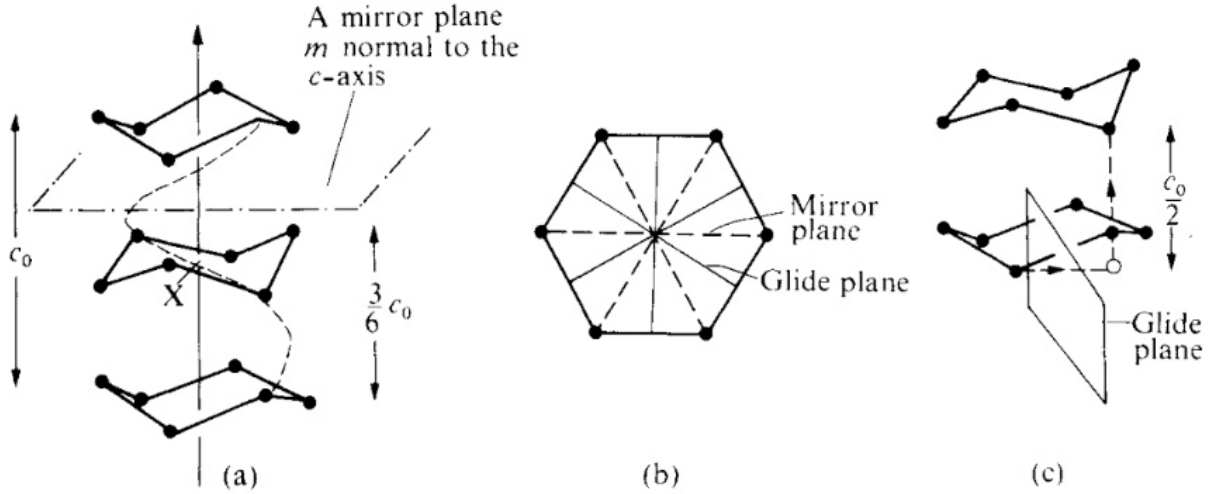

Figure 3: The symmetry elements of ice Ih a) the screw axis 6_3 and a mirror plane *m* normal to the c-axis. b) Mirror planes *m* and glide planes *c* parallel to the c-axis. c) Operations of a glide plane. [Hobbs, 1974]

The Ih lattice has only the c-axis as the major axis of symmetry. This accounts for the fact that the physical properties (thermal conductivity, elastic stiffness and atomic diffusivity) are isotropic (radial isotropic) in all directions perpendicular to the c-axis. [Schulson and Duval, 2009].

The density of ice can be deduced from the lattice parameters and from the fact that there are four molecules per unit cell [Schulson and Duval, 2009]. Table 1 lists values of the density of ice Ih as a function of temperature under atmospheric pressure deduced from diffraction measurements of the unit cell parameters [Hobbs, 1974]. The value of the density at 0°C obtained using the hydrostatic weighing method on glacier ice single crystals [Bader, 1964] is in agreement with the value in Table 1. The higher the pressure on the ice the higher the density [Gagnon et al., 1988]. Over the temperature range -30°C to 0°C, Gammon et al. (1983) also expressed the temperature dependence of the density of ice in an equation.

Table 1: Density of ice Ih as a function of temperature under atmospheric pressure [Hobbs, 1974]

Temperature (°C)	**Density (kg m^{-3})**
0	916.4
-30	919.3
-60	922.7

The reason for a decrease of density is an increase of the O-O distance [Dantl, 1968]. The spacing between the oxygen atoms is large relative to the size of the atoms themselves. Consequently, there is a large amount of open space within the lattice. This openness accounts for ordinary ice being less dense than water. It accounts also for the pressure-induced reduction of the melting point [Schulson and Duval, 2009].

2.2 Crystallographic defects

A perfect crystal is an idealization. Atom arrangements in real materials do not follow perfect crystalline patterns. The preferred structures of solids at low temperatures are those that minimize the energy. The low-energy atomic configurations are almost invariably crystalline since the regular pattern of the crystal lattice repeats whatever local configuration is most favourable for bonding. There is also a fundamental physical reason, why the crystal is imperfect. While a perfect crystalline structure may be preferred energetically, at least in the limit of low temperature, atoms are relatively immobile in solids. Therefore, it is difficult to eliminate whatever imperfections are introduced into the crystal during its growth, processing or use. The most important features of the microstructure of an engineering material are the crystalline defects [Morris, 2007]. In ice, many of the mechanical properties are determined by them [Hobbs, 1974].

In this subchapter, the various defects of ice will be identified and described briefly. They are classified by their dimension [Morris, 2007]:

2.2.1 Point defects

These 0-dimensional defects are atomic-sized features, which form inter alia vacancies, interstitials and solutes in the ice lattice [Morris, 2007; Schulson and Duval, 2009].

2.2.2 Line defects: dislocations

These 1-dimensional defects are called dislocations, which are line defects within the crystal lattice [Morris, 2007]. They are created during thermal-mechanical history of the material and are fundamental to plasticity and strength. Dislocations may be viewed as the boundary between the slipped and the un-slipped part of the crystal [Schulson and Duval, 2009]. Crystals commonly contain three types of dislocations:

- edge dislocations (Figure 4 b) and e));
- screw dislocations (Figure 4 d) and g));
- mixed dislocations (Figure 4 c) and f)), they are the most common type and mixture of edge and screw types.

Dislocations are fundamental to crystal plasticity, because they allow slip to occur under applied shear stress. Dislocation generate an internal shear strain that partially bends atomic bonds within the vicinity of core. Once dislocations emerge, the multiply as they glide, leading in the end to a greater dislocation density as in the beginning [Schulson and Duval, 2009] and the crystal is weakened [Michel, 1978].

2.2.3 Planar defects

The 2-dimensional defects are called planar defects. They are surfaces, such as the external surface and the grain boundaries [Morris, 2007].

Grain boundaries are nanometre-wide regions within polycrystals that separate individual grains or crystals. In common they have a difference in orientation of >10°, which is also taken to define a high-angle boundary [Schulson and Duval, 2009]. High-angle boundaries generally contain ledges and facets, from several tens of microns up to 1 mm heights [Liu et al., 1995]. Near the melting point, grain boundaries contain liquid water in sub-millimetre-sized veins that lie along lines of intersections [Nye, 1992].

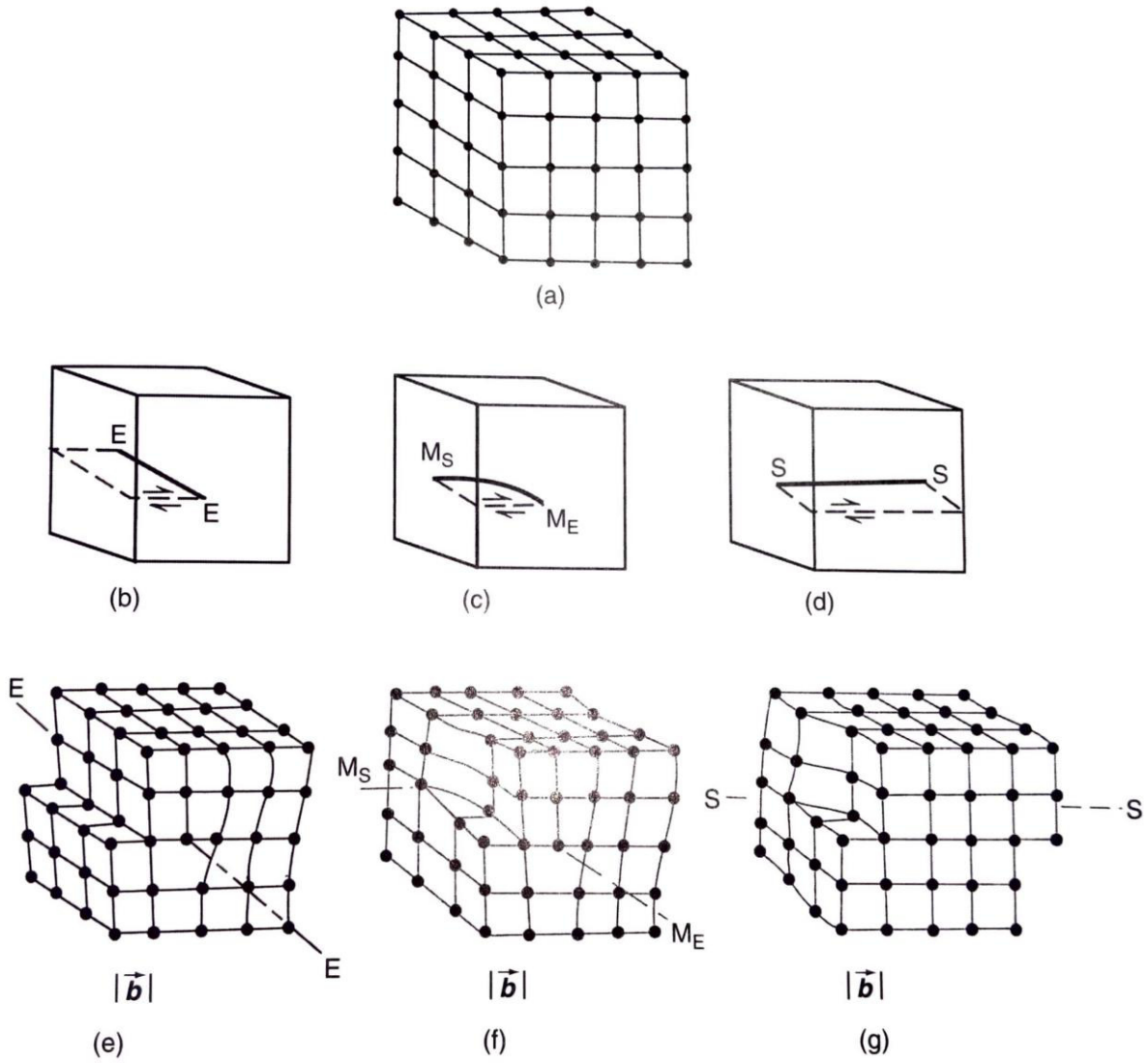

Figure 4: Schematic sketches of dislocations in hypothetical simple cubic crystal. a) The perfect crystal. b) and e) edge dislocation EE; c) and f) mixed dislocation M_S and M_E; d) and g) screw dislocation [Schulson and Duval, 2009]

2.2.4 Volumetric defects

The 3-dimensional defects change the crystal pattern over a finite volume. They include precipitates, which are small volumes of different crystal structure, and include large voids or inclusions of second-phase particles [Morris, 2007].

In ice the most common volumetric defect are pores. When ice is made through solidification, pores form as result of rejecting oxygen and nitrogen from water and the ice lattice. Within fresh-water ice, they contain air only. Pores tend to lower the resistance to creep deformation [Schulson and Duval, 2009].

3 Physical and mechanical properties of ice

In this chapter, the physical and mechanical properties of ice will be discussed. Therefore, the elastic behaviour of intact ice and cracked/damaged ice will be analysed. With that, numerical values for both single crystals and polycrystals will be presented.

3.1 Elastic properties of ice Ih single crystals

When a solid body is subjected to a stress, its shape changes. The body deforms elastically, when it returns to its original shape when the stress is removed [Hobbs, 1974]. When ice is deformed elastically, it follows Hooke's law. The strain ε is proportional to the applied stress σ, so that:

$$\varepsilon = S \cdot \sigma \tag{1}$$

where S is the compliance constant if ice. With the stiffness constant C, this equation may also be written [Michel, 1978]:

$$\sigma = C \cdot \varepsilon \tag{2}$$

Both, stress and strain are specified by second-order tensors, and so S and C are specified by fourth-order tensors. Generally, the constants are given as components of 6 x 6 matrices. The elastic behaviour may then be written as following:

$$\varepsilon_i = S_{ij} \cdot \sigma_j \tag{3}$$

$$\sigma_j = C_{ij} \cdot \varepsilon_i \tag{4}$$

where S_{ij} and C_{ij} denote the components of the matrices and i and j take integral values from 1 to 6 inclusive [Hobbs, 1974; Schulson and Duval, 2009].

These constants are expresses with respect to a rectangular coordinate system whose axes are specified in terms of the unit cell of the crystal. The axes of the principal stress and principal strain are coincident. On this basis the elastic compliance constant may be interpreted as follows:

- S_{11} gives the normal strain perpendicular to the c-axis;
- S_{33} gives the normal strain parallel to the c-axis owing to a normal stress acting along c-axis;
- S_{12} gives the normal strain perpendicular to the c-axis owing to a normal stress perpendicular to the c-axis and perpendicular to the direction of interest;

- S_{13} gives the normal strain perpendicular to the c-axis owing to a normal stress acting along the c-axis and perpendicular to the direction of interest, as well as the normal strain along the c-axis owing to a normal stress perpendicular to the c-axis;
- S_{44} gives the shear strain in a plane parallel to the c-axis owing to a shear stress in the same plane [Schulson and Duval, 2009].

It can be seen that the numerical value of the strain and stress constants depends on the orientation of the c-axis in the single crystal and the direction of the stress.

One of the physical characteristics of ordinary ice is radial isotropy. Isotropic ice can become anisotropic with development of texture [Schulson and Duval, 2009]. However, for a material that is isotropic in its elastic behaviour, following can be said [Hobbs, 1974]:

$$E = \frac{1}{S_{11}} \tag{5}$$

$$\nu = -\frac{S_{12}}{S_{11}} \tag{6}$$

$$B = \frac{1}{S_{11} + 2S_{12}} \tag{7}$$

$$G = \frac{1}{2(S_{11} + S_{12})} \tag{8}$$

The Young's modulus (modulus of elasticity) E is the stiffness constant. When a tensile or compressive force is applied to a body, the tensile stress is equal to the force acting on a unit area of the body normal to the direction of the force; the longitudinal strain is the fractional increase in the length of the body in the direction of the applied force.

The Poisson's ratio ν is the ratio of the longitudinal strain along the directions of a tensile force to the strain produced in a direction perpendicular to the force.

The bulk modulus B is the stiffness constant, the ratio of the applied pressure to the fractional change in the volume of the body, when a pure compressional stress is applied its volume will change. The reciprocal of the bulk modulus is the compressibility K.

Under shear stress, a body will suffer shear strain. The stiffness constant is then referred to as the shear modulus (rigidity modulus) G [Hobbs, 1974; Michel, 1978].

Gold (1958) found that in temperature range -3 to -40°C ice behaves as an almost perfect elastic body and Hooke's law is obeyed, provided there is maximum stress of 10 bar, a rate of stressing of 5 bar s^{-1} and with a duration of stress less than 10s.

Altogether there are, because for an isotropic body, only two independent elastic parameters [Hobbs, 1974]. A quantity of interest is Young's modulus in an arbitrary direction. Just as the strain and stress constants, the numeric value of all other elastic parameters vary with direction of loading too. For any direction the compliance constants can be obtained from an equation by Fletcher (1970).

$$S_\alpha = S_{33} \cdot \cos^4 \alpha + S_{11} \sin^4 \alpha + (S_{44} + 2\, S_{13}) \sin^2 \alpha \cos^2 \alpha \tag{9}$$

Where the S's are the compliance constants and α is the angle between the direction of loading and the c-axis. The Young's modulus of ice is the reciprocal to the corresponding compliance constant [Michel, 1978]. It reaches a minimum at α~50° of E = 8.42 GPa at -16°C. This compares with highest value E(0) = 11.8 GPa along the c-axis and with E(90) = 9.71 GPa along any direction within the basal plane. These differences are relatively small and indicate that the elastic behaviour of ice Ih is only moderately anisotropic [Schulson and Duval, 2009]. In Figure 5 the Young's modulus E of ice Ih single crystal at -16°C is shown as a function of the orientation of the loading direction with respect to the c-axis [Michel, 1978].

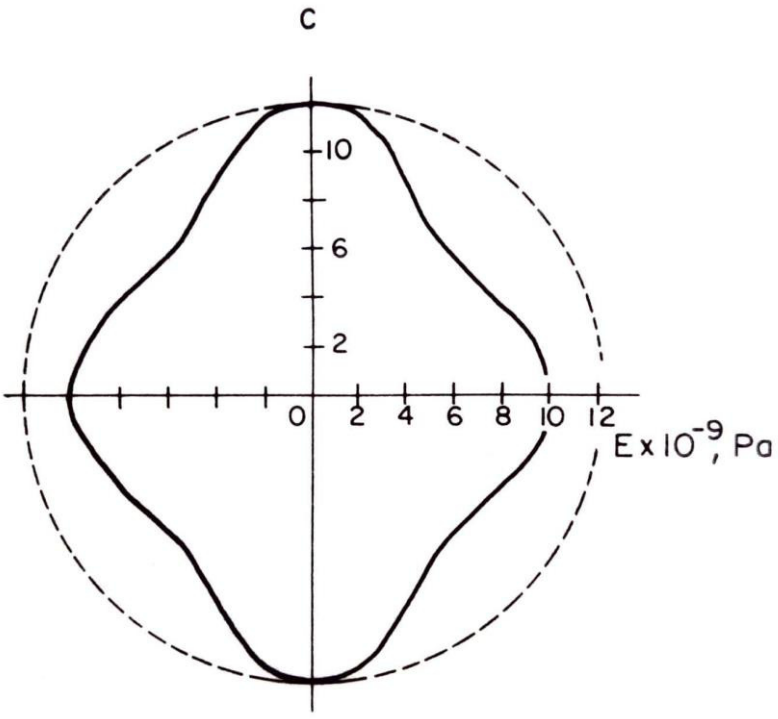

Figure 5: Young's modulus E of ice Ih single crystal as a function of the orientation of the loading direction with respect to the c-axis [Michel, 1978].

Two different approaches have been taken to measure the elastic properties of ice. The measurement of displacement under an applied stress (*static* method), is the simpler, but more problematic approach. Because creep (time-dependent deformation) contributes to the deformation, unless the stress is low and is applied and then released very rapidly. This leads

to an underestimate of stiffness or overestimate of compliance [Hobbs, 1974; Schulson and Duval, 2009]. Also, it is known that the apparent Young's modulus, when measured from the slopes of stress strain curves from single crystals, is a factor of two lower than the true elastic modulus [Schulson and Duval, 2009]. For this reason, the elastic constants deduced from high frequency measurements (*dynamic* values), where the propagation of sound waves are exploited, are more reliable [Hobbs, 1974; Schulson and Duval, 2009].

For ice, many authors have determined the static and dynamic elastic constants. The most accurate values to date have been obtained by Gammon et al. (1983) with the method of Brillouin spectroscopy. In Table 2, numerical values for dynamic elastic parameters for ice Ih single crystals at -16°C are given.

Table 2: Elastic constants for ice Ih single crystals at -16°C [Gammon et al., 1983]

Property and units	**Symbol**	**Value**
Elastic stiffness (10^9 N m^{-2})	C_{11}	13.93 ± 0.04
	C_{12}	7.08 ± 0.04
	C_{13}	5.78 ± 0.02
	C_{33}	15.0 ± 0.05
	C_{44}	3.01 ± 0.01
Elastic compliance (10^{-12} m^2 N^{-1})	S_{11}	103 ± 0.05
	S_{12}	-42.9 ± 0.4
	S_{13}	-23.2 ± 0.2
	S_{33}	84.4 ± 0.4
	S_{44}	331.8 ± 0.2
Bulk modulus (10^9 N m^{-2})	B	8.90 ± 0.02
Poisson's ratio	ν	$\nu_{12} = -S_{12}/ S_{11} = 0.415$
		$\nu_{12} = -S_{13}/ S_{11} = 0.224$
		$\nu_{12} = -S_{13}/ S_{33} = 0.274$

Both, E and G depend only on the angle between the crystal axis and the c-axis. This means that the elastic properties of ice Ih are invariant with respect to rotation about the c-axis [Schulson and Duval, 2009].

3.2 Elastic properties of ice Ih polycrystals

Almost all crystalline solids are polycrystalline. They are composed of many small crystallites (grains) of the primary constituent, and may also contain several distinct constituents (phases) of different composition and crystal structure. The interfaces that separate grains are called grain boundaries. Those that separate phases are called two-phase interfaces (Figure 6) [Morris, 2007].

Polycrystalline ice consists of several single ice crystals, which are separated by grain boundaries. The structure of a grain boundary depends on the misorientation of the crystal grains that it separates. When the misorientation is small, the boundary is a reasonably simple planar array of dislocations and then being called a low-angle boundary. When the misorientation is larger, the boundary structure is more complicated. Then it is often useful to picture the boundary as simply a region of disorder between the two crystal grains [Morris, 2007]. The elastic properties of polycrystals free from porosity and other defects can be calculated from the fundamental elastic constants and from orientations, sizes and shapes of grains, using number of different methods [Schulson and Duval, 2009], as long as the number of grains exceed about 230 [Elvin, 1996].

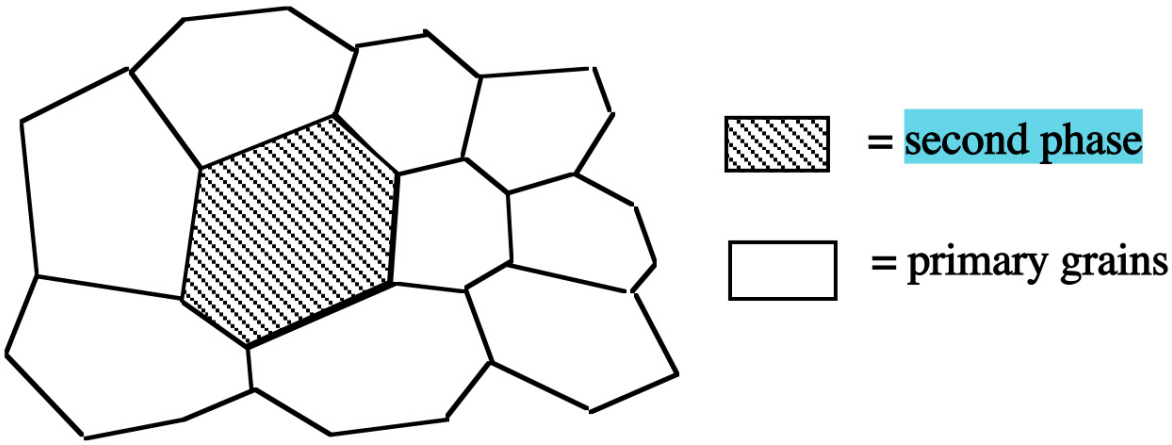

Figure 6: Schematic drawing of polygranular grain structure showing [Morris,2007]

In isotropic polycrystalline ice, the grains are randomly oriented with respect to one another [Durham and Stern, 2001] and anisotropic properties of ice single crystals are filled in [Häusler, 1989]. Although the constituent crystals are anisotropic, isotropic polycrystalline ice is elastically isotropic [Schulson and Duval, 2009]. Therefore, two independent constants chosen from the Young's modulus E, the Poisson's ratio ν, the bulk modulus B and the shear modulus G are enough to describe their elastic properties [Gammon et al., 1983]. For example [Schulson and Duval, 2009]:

$$G = \frac{E}{2(1+\nu)} \tag{10}$$

and

$$B = \frac{E}{3(1-2\nu)}. \tag{11}$$

In Table 3, the numerical values of elastic parameters of homogeneous polycrystals of isotropic ice Ih at -16°C are given [Gammon et al., 1983].

With V(T) as the value of any of the fundamental constants at temperature T and T_r the room temperature, the effect of temperature may be obtained as follows [Schulson and Duval, 2009]:

$$V(T) = V(T_r)[1 \pm 1.42 \cdot 10^{-3}\ (T - T_r) \tag{12}$$

Table 3: Elastic parameters of homogeneous polycrystals of isotropic ice Ih at -16°C [Gammon et al., 1983]

Property and units	**Symbol**	**Value**
Young's modulus (10^9 N·m^{-2})	E	9.332
Shear modulus (10^9 N·m^{-2})	G	3.521
Bulk modulus (10^9 N m^{-2})	B	8.899
Poisson's ratio	ν	0.325

The porosity of the solid has a critical influence on elastic properties of ice. The porosity is a fraction of the volume of voids over the total volume. Voids in ice cause a decrease of the stiffness [Schulson and Duval, 2009] and the strength [Weeks and Assur, 1967; Michel, 1978].

3.3 Cracks

Cracks form in ice during deformation and/or as a result of thermal straining, they reduce stiffness. When induced by deformation, they tend to be oriented, parallel to direction of the greatest applied stress under compression [Schulson and Duval, 2009]. Following made

predictions are expectations by Schulson and Duval (2009), based on a model. Still, they need to be tested through experiments.

The crack-free polycrystalline ice is elastically isotropic. However, the elastic behaviour of cracked ice may be described in a manner similar to that used to describe the behaviour of Ih single crystals. Because when compressed to the extent that along the direction of maximum compressive stress an axis-symmetric array of cracks develops, the three-dimensional isotropy is degraded, but transverse isotropy remains. [Schulson and Duval, 2009].

4 Principles of ultrasonic testing and processes

Testing with ultrasonic is a classical test method in the non-destructive material testing. The ultrasonic principle is based on the fact, that solid materials are good conductors of ultrasonic waves [Berke, 1996]. The reason for this is that ultrasonic waves consist of mechanical oscillations, which are linked to material appearance [Tietz, 1974]. The smaller the wavelength, the stronger the interaction effect of sound waves with the material and the higher the frequency of the wave [Berke, 1996]. Ultrasonic has a frequency range from 16 kHz up to 1 GHz [Millner et al., 1987].

Figure 7 shows the instantaneous picture of a section of the model in which a wave travelling from left to right has not yet reached the right edge. It can be seen that the phase shift of the oscillations creates zones, where the particles approach each other particularly closely. These compression zones alternate with dilated zones. The chronological pattern of the wave shows that these zones are constantly recreated on the excitation side and that they travel in the body at constant velocity and uniform intervals towards the right. This represents an elastic wave [J. Krautkrämer and H. Krautkrämer, 1990].

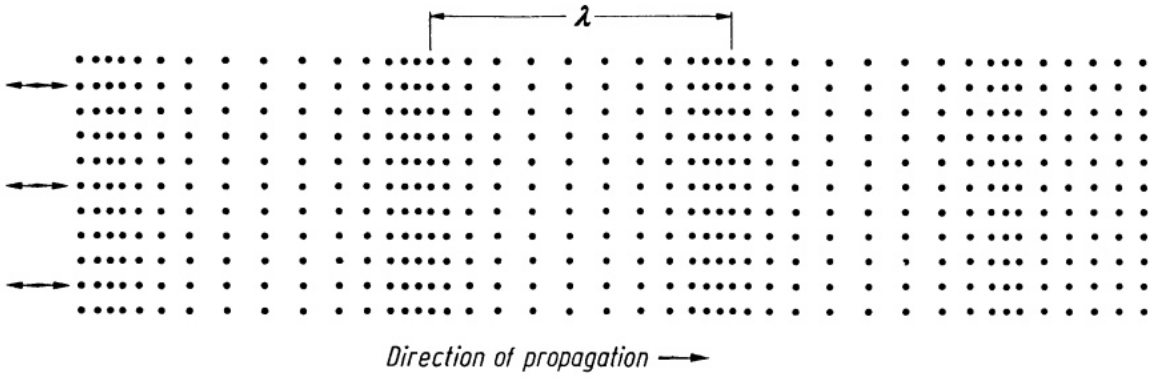

Figure 7: Longitudinal wave [J. Krautkrämer and H. Krautkrämer, 1990].

By reference to equation (13), some parameters of a wave will be defined. The *frequency* f of a wave is the number of oscillations of a given particle per second. It is the same for all particles within a wave. The frequency of the generator, which can be chosen arbitrarily, is identical with the frequency of the wave. The *wavelength* λ is the distance between two planes in which the particles are in the same state of motion, for instance two compression zones (Figure 7) [J. Krautkrämer and H. Krautkrämer, 1990]. The relation between the wavelength and the frequency is given as following [Tietz, 1974]:

$$\lambda = \frac{c}{f}. \tag{13}$$

The *sound velocity* c is the velocity of propagation of a given state, for example a dilated zone. It is a substance property and in general a constant for a given material for any frequency and any wavelength. The pressure in a given sound field is called *sound pressure*. It is the alternating pressure, when a very small and inertia less pressure gauge placed in the path of the sound wave, would indicate alternately high pressure and low pressure in a sinusoidal sequence. In the dilated zones, the pressure is likewise lower than the normal pressure, than at points of higher particle density it is. The *amplitude of the sound pressure* is the maximum deviation from the normal pressure (without sound wave) [J. Krautkrämer and H. Krautkrämer, 1990].

The *longitudinal* and *transversal* wave are two fundamental types of waves concerning the propagation direction. In the event of *longitudinal wave*, oscillations occur in the direction of propagation (Figure 7). In solid materials, it exists of periodically changes of the principal stress. In case of the *transversal wave,* the particles oscillate at right angles to the direction of propagation [Millner et al., 1987]. In Figure 8, the transversal wave is shown schematically in the form of an instantaneous picture of the particle motion. It will again be assumed that the wave travels from left to right. The excitations can be visualised as a motion in which the particles on the left surface of the body are moved sinusoidally up and down by a periodical shear force. For the practical testing of materials, transversal waves can penetrate appreciable distances only in solid bodies, because gases and liquids are in practice incapable of transmitting shear. [J. Krautkrämer and H. Krautkrämer, 1990].

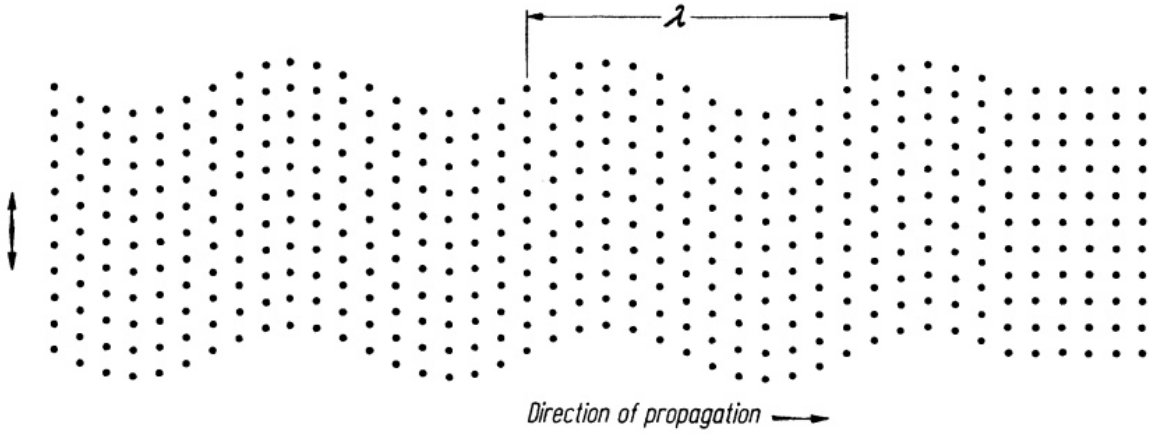

Figure 8: Transversal wave [J. Krautkrämer and H. Krautkrämer, 1990].

4.1 Generation and detection of ultrasonic waves

Regarding the propagation and emission, ultrasonic waves are subjected to the same physical principles as other mechanical oscillations [Tietz, 1974]. A wave can be analysed only theoretically in an infinitely extended substance, because every substance has a boundary and ends somewhere. At the boundary, the propagation of the wave is disturbed, because the transmission of a wave always requires the presence of particles of material. If the material concerned borders on an empty space, no wave can go beyond this boundary because the wave may return in some way. At a rough boundary this phenomenon is called *scattering*, and at a smooth boundary *reflection* [J. Krautkrämer and H. Krautkrämer, 1990]. Therefore, waves are not only reflected by interfaces, but also by internal flaws (defects) [Berke, 1996]. If another material, beyond the boundary, adheres to the first material so that forces can be transferred, the wave can be propagated in a more or less changed direction, intensity and mode, into this material [J. Krautkrämer and H. Krautkrämer, 1990]. This phenomenon is called *transmission*. [Millner et al., 1987].

For instance, a plane wave incident on a perpendicular, flat, smooth boundary. Only plane waves can then be propagated at right angles to the boundary. Here, this is a reflected wave, which opposes the incident wave, and a transmitted wave [J. Krautkrämer and H. Krautkrämer, 1990]. However, if a plane wave incident on an oblique oriented surface, during the reflection it will be split into a longitudinal and a transversal wave [Tietz, 1974].

The contact face of a radiator, which oscillates with the desired waveform and frequency, excites ultrasonic waves in the material. The waves are detected by a contact face, which

measures the sound pressure of an incident wave [J. Krautkrämer and H. Krautkrämer, 1990]. For the measurement of solid bodies, the radiator should have a high efficiency and be able to generate high frequencies. Therefore, the principle of operation of the radiator is based on the piezo-electricity [Tietz, 1974]. The radiator is called *transmitting probe*, the receptor is called *receiving probe*. The transmitting probe may serve as a receiving probe at the same moment. In general, both can be referred to as a *probe* or *transducer* [J. Krautkrämer and H. Krautkrämer, 1990].

In any ultrasonic test, a direct contact between the test surface and probe is required. In practical, it is not possible to create a surface free from roughness. Therefore, always a gap is present between surface and probe. In order that a sound-conducting contact between the rough test surface and the probe exists, a coupling media is required. For the coupling media, water, oil, gel or glycerine may be used [Tietz, 1974]. A disadvantage of water is, that it is not wetted satisfactorily, which is an important requirement for good coupling. However, by adding a wetting agent, water is a very useful coupling media either in the form of a constant flow of water between probe and surface or as a stationary layer on horizontal surfaces [J. Krautkrämer and H. Krautkrämer, 1990].

4.2 Methods of ultrasonic testing of materials

In this section, some ultrasonic testing methods will be described. J. Krautkrämer and H. Krautkrämer (1986; 1990) categorized the methods by their primary measured quantity and the form of radiated ultrasound used (continuous wave or pulses) and outlined them in the following way.

The most important method is the *pulse-echo method*. A material inhomogeneity, when illuminated by a pulsed ultrasonic beam, reflects an echo that is picked up by a receiver probe (Figure 9). Therefore, the primary measured quantities are the amplitude of the sound pressure and the transit time of the pulse from the transmitter to the reflector and back.

A probe generates an ultrasonic pulsed wave and propagates it into a specimen with the ultrasonic velocity corresponding to the respective material. At obstacles in the form of an inhomogeneity, a part of the ultrasound will be reflected. If the obstacle is not too large, the remaining ultrasound will travel further to a boundary of the specimen, where it will be reflected, in the transit time of the pulse between the receiver and the back wall, back to a receiver, too. Therefor the receiver should be in favourable position to the receiver. The signal obtained from the receiver is displayed as a peak on a base line of a cathode ray tube. The

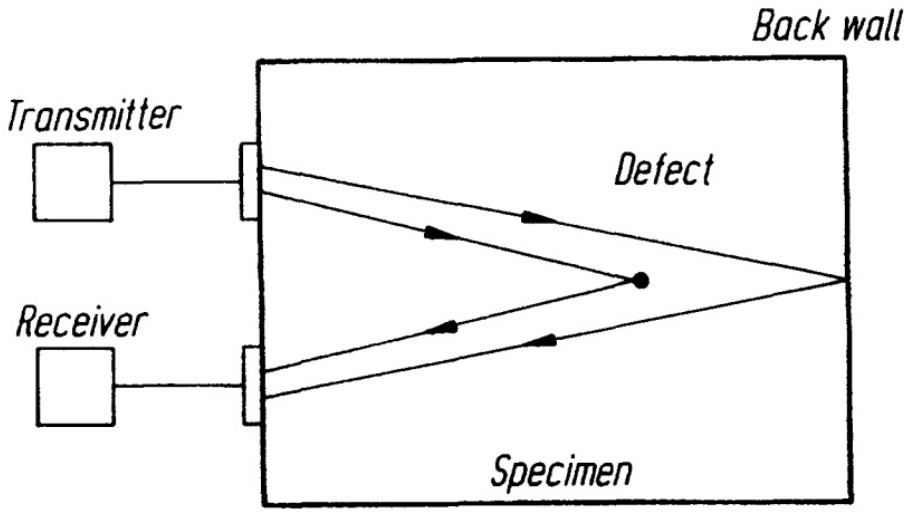

Figure 9: Principle of the pulse-echo-method [J. Krautkrämer and H. Krautkrämer, 1990]

horizontal sweep is proportional to the time. If the boundaries of the specimen are plane parallel, an image similar to Figure 10 can be seen. To obtain a standing image the pulses and the sweep of the cathode ray tube are synchronised at the so-called pulse-repetition frequency.

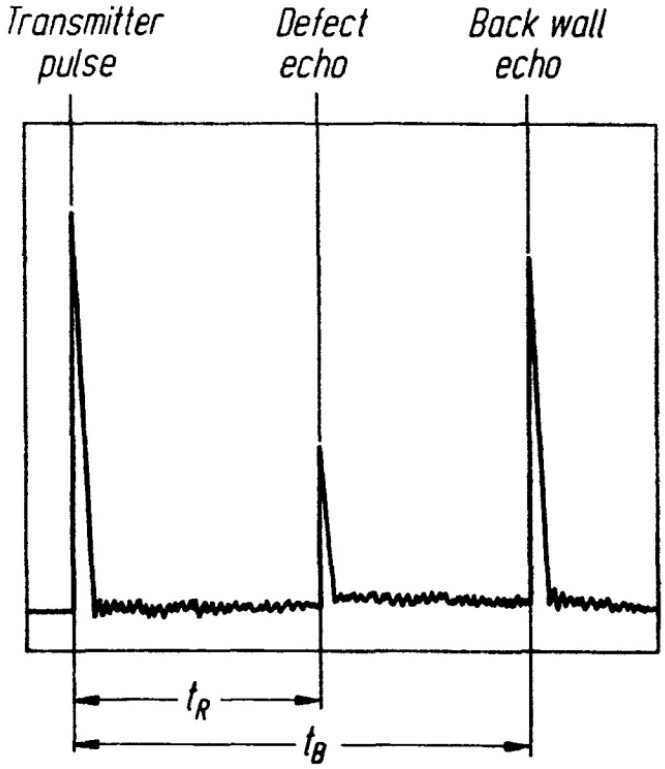

Figure 10: Display on the cathode ray screen [J. Krautkrämer and H. Krautkrämer, 1990]

By reading the transit times t_R and t_B to the reflector and defect respectively the back wall from the screen, knowing the velocity of sound c and the base line in time per unit length, we obtain for the distance e of any reflector:

$$e_i = \frac{c \cdot t_i}{2} \tag{14}$$

The thickness d_B can be determined by measuring the distance between start and the back wall of the specimen. Now, the sweep can be calibrated directly in units of length. Because the horizontal sweep is proportional to the time, the exact position of the defect can be seen on the display in units of length.

In an example, a specimen of 100 mm thickness is tested and its back echo is positioned at the right-hand edge of the screen (100%) by varying the velocity of the ultrasound. An indication of a defect appears at 30 % of the distance of the back echo, which means that the reflection took place at a depth of 30 mm from the surface. In this way, a scale can be placed in front of the screen, and the beginning of the transmitter peak and the back-wall echo peak shifted respectively to the zero and the 100 mm points.

Several defects can be indicated simultaneously, assumed none of them is masked by another defect. Because of the reflection on each of the parallel boundaries, a sequence of multiple back echoes will be shown at the cathode ray screen (Figure 11). Furthermore, the amplitude of the received echo depends on several influences. they include:

- Transmitter pulse power entering the specimen,
- Directivity of the transmitter probe,
- Size of the reflector,
- Surface quality of the reflector,
- Position of the reflector,
- Size and directivity of the receiver probe,
- Losses at the receiver by reflection and coupling,
- Attenuation of the wave by absorption and scattering of the material.

Some of them are illustrated in Figure 12.

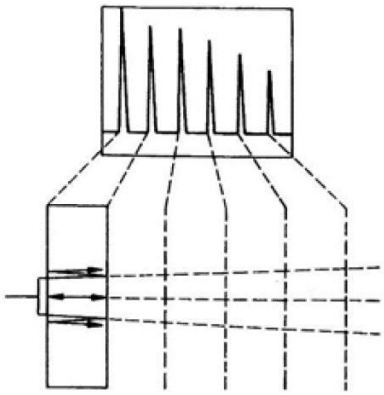

Figure 11: Schematic screen with multiple echoes in a plate [J. Krautkrämer and H. Krautkrämer, 1990].

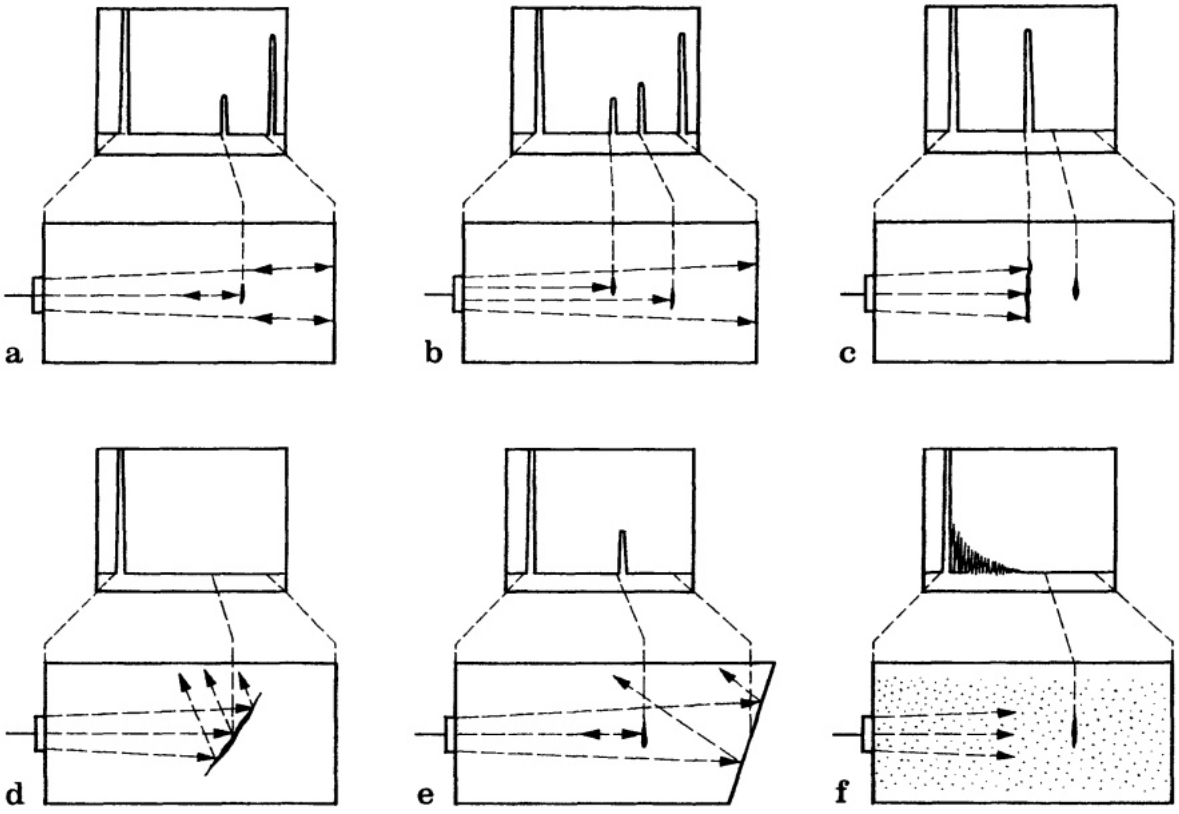

Figure 12: Schematic screen pictures obtained by the pulse-echo method. a) Small flaw in sound beam; b) two small flaws in sound beam; c) large flaw in sound beam, smaller second flaw and back wall masked; d) large, obliquely orientated flaw, back wall masked; e) small flaw, but no back wall echo because of the obliquely orientated back wall; f) no echo from flaw or back wall due to scattering of material [J. Krautkrämer and H. Krautkrämer, 1990].

In the *transit-time method*, the amplitude of the sound pressure only needs to reach a minimum detectable value. The primary measured quantity is the transit time, or a

corresponding frequency. An information about the amplitude of the sound pressure is not necessary here. With this method, mainly the wall thickness is evaluated. In other types of the transit-time method, continuous ultrasound is used instead of pulses, in which inhomogeneities of the material also act as reflectors.

In the *shadow method*, an inhomogeneity between transmitter and the opposing receiver produces a shadow that influences the sound amplitude, as known from X-ray diagnostics. The primary quantity to be measured is the amplitude of the sound pressure. This method can be used either with pulses or with continuous sound. Historically the latter variant was the first ultrasonic testing method used in an attempt to imitate X-ray screening. After having located a defect it is of great importance to make a statement about its size. Its shadow could be very useful, as revealed by X-ray screening. The aim of all *imaging methods* is the optical visualization of structures, which in other ways could not be seen. By the use of sound sensors, signals are obtained to transform the acoustic 'picture' into a visual image.

The *sound emissions analysis* is not much applicable; just few norms respectively suggestions for norms exist. However, this method precisely presupposes a destruction, namely the widening of a crack. In future, this may be interesting for the measurement of cracks in ice.

With a growing crack or from deformation stresses within the specimen, energy is released in the form of sound waves. A receiver as a pulse counter registries single pulses per second. Growing cracks then are indicated by a rising pulse rate. In some circumstances, certain conclusions about the behaviour of the material and its failure are possible. With particular techniques and the usage of more than one receiver probe, it is even possible to determine the position of the crack.

4.3 Ultrasonic testing by determination of mechanical properties

This section deals with the measurement of sound velocity and mechanical properties. In a sound permeable material, the ultrasonic measurement gives the opportunity to measure the Young's modulus E, the Poisson's ratio ν and the shear modulus G on a non-destructive and a relatively easy way [Tietz, 1969]. In chapter 3.2 the relation between the elastic constants is given. Thereby it is necessary, that two constants are independent and the material is isotropic. As a function of the acoustic longitudinal wave velocities c_l, the transversal wave velocities c_t, and the density ρ, the elastic constant can be described as following [Tietz, 1969; J. Krautkrämer and H. Krautkrämer, 1986]:

$$E = 4 \cdot \rho \cdot c_t^2 \cdot \frac{\frac{3}{4} - \left(\frac{c_t}{c_l}\right)^2}{1 - \left(\frac{c_t}{c_l}\right)^2}, \tag{15}$$

$$G = \rho \cdot c_t^2 \tag{16}$$

and

$$\nu = \frac{\frac{1}{2} - \left(\frac{c_t}{c_l}\right)^2}{1 - \left(\frac{c_t}{c_l}\right)^2}. \tag{17}$$

From this it follows, that

$$E = 2G \cdot (1 + \upsilon), \tag{18}$$

so, that

$$E = \rho \cdot c_l^2 \cdot \frac{(1 + \upsilon) \cdot (1 - 2\upsilon)}{1 - \upsilon}. \tag{19}$$

The measurement of velocities of sound has great practical importance and various methods can be used for their determination. Using a pulse-echo instrument, the measurement accuracy is determined by the calibration accuracy of the instrument. In general, this will not be better than about 1 % [J. Krautkrämer and H. Krautkrämer, 1990]. The instrument has to be calibrated for a definite velocity of sound c; an unknown velocity of sound c_x can be determined by measuring the thickness d_x of the specimen. The true thickness d has been determined by mechanical measurement, we then have [J. Krautkrämer and H. Krautkrämer, 1990]:

$$c_x = c \cdot \frac{d}{d_x}. \tag{20}$$

5 Operating the ultrasonic unit Krautkrämer USD 10

All measurements are performed with the ultrasonic test unit Krautkrämer USD 10 (1986 model; Figure 13) and two vertical probes Karl Deutsch S12W4 (Figure 14) in the laboratories of the Institute for Ship Structural Design and Analysis of Hamburg University of Technology. For the calibration and measurement with the unit, the operating instruction TUHH-B3-AA111 by Schmidt-Döhl (2014) and the USD10 basic operation guide (n.d.) were used.

Figure 13: Ultrasonic test unit Krautkrämer USD 10

Figure 14: Vertical probe Karl Deutsch S12W4

5.1 Calibration

To calibrate the unit and the probes, the probes have to be connected with the unit. After the unit is turned on and the initializer takes place, some preliminary settings have to be carried out. For the cylindrical calibration body dependent on the P-wave, following information is given [Schmidt-Döhl, 2014]:

Table 4: Properties of the calibration body [Schmidt-Döhl, 2014].

Property and units	**Value**
Length (mm)	109.5
Sound velocity ($m \cdot s^{-1}$)	4200
Transit-time standard of the P-wave µs	26

With the calibration body, the parameters of the unit will be adjusted, so that the right transit-time of the impulse will be shown. These parameters will then be applied in every measurement, with the above-mentioned probes [Schmidt-Döhl, 2014]. For measurements with two Karl Deutsch S12W4 probes in transmission, following appropriate settings and values in the menu point GRUNDFUNKTION can be adopted [Schmidt-Döhl, 2014]:

Table 5: Settings and values in the menu point GRUNDFUNKTION [Schmidt-Döhl, 2014].

Parameters	**Settings and Values**
BILD-ANF	0.000 mm
BILD-BREIT	*Higher than the length of the specimen; For the calibration body* 120.0 MM
V-SCHALL	04200 M/S *is the longitudinal sound velocity in the calibration body For other material other values are shown..*
PK-VORL.	*Has specifically to be calibrated for the probes.*
FREQ.	4.0 MHz
GLEICHR.	POS.HW

INTENS.	4
PK.ANP	75 OHM
S/E	EIN
UNTERDR	00%
A-MODE	KOINZID.
A-SCHWEL	20%
A-ANFANG	*Start of the local axis, supposed to be smaller than the back wall echo;* for the calibration 54.00 MM
A-BREITE	*Latitude of the local axis, adjust it so that the back wall echo can be seen sufficient*; for the calibration 02.00 MM
LUPE	BLENDE*, if zoom function shall be activated, else* AUS.
ABB.HALT	EIN*, if image shall be freeze, else* AUS.

In the menu point of JUSTIERFUNKTION, FOLLOWING adjustment will be done [Schmidt-Döhl, 2014]:

Table 6: Settings and values in the menu point GRUNDFUNKTION [Schmidt-Döhl, 2014].

Parameter	**Settings and Values**
MESS-ART	FLANKE

After the parameters in the unit have been adjusted, the practical part of the calibration starts. Therefor the transmitting probe and the receiving probe are coupled with a coupling media to respectively each plane surface of the calibration body. The coupling media, ECHOTRACE - Couplant for Manual Ultrasonic Testing, a fragrant gel based on water, is applied as a thin layer on the complete contact surface. The probes are held at the centre of the surface of the calibration body. Now, the back wall echo in form of a pulse is screened at the display, as shown in Figure 15. The gain is increased by the button dB, so that the back wall echo can preferably make use of the whole display. Next, the function LUPE will be adjusted to BLENDE A. Thus, an extended excerpt will be gained [Schmidt-Döhl, 2014].

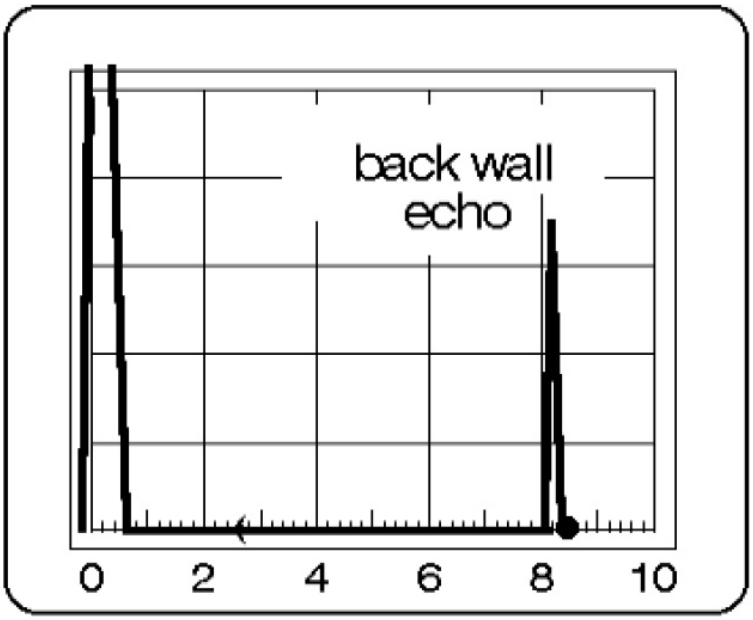

Figure 15: Schematic screen with back wall echo [Berke, 1996]

To complete the calibration, PK-VORL. has to be calibrated for the Karl Deutsch S12W4 vertical probes. The unit is set for reflection measurements, where the distance from one surface to the back wall and the return distance from back wall to surface is measured (Figure 16). But because we measure with two probes at respectively each plane surface, the probe delay PK-VORL. should be adjusted to a value, where only half of the length of the calibration body (54,75 mm) is displayed on the screen. Consequently, the value of the probe delay comes to 1.460 US. After the completion of the calibration, measurements with specimen can be started.

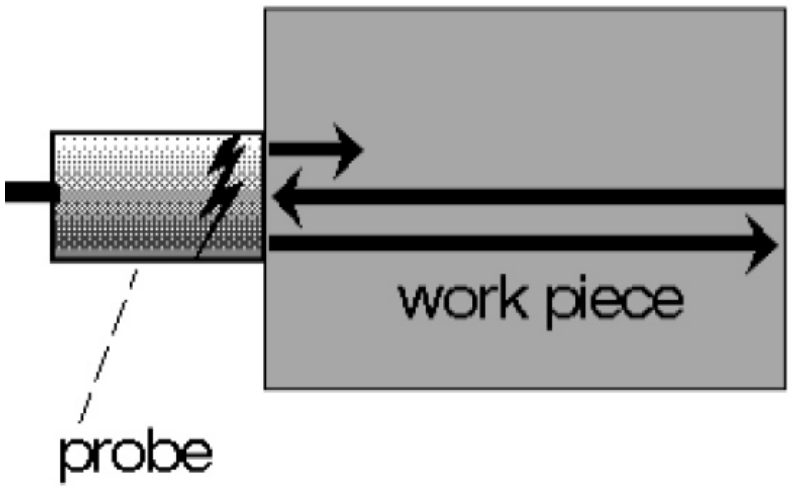

Figure 16: Schematic reflection measurement with one probe [Berke, 1996]

5.2 Measurement of the Young's modulus of steel

Before the tests with ice specimen start, the above-mentioned methods were applied on a cubic 42CrMo4 steel specimen, with an edge length d = 45 mm, to measure its Young's modulus with equation (19):

$$E = \rho \cdot c_l^2 \cdot \frac{(1+v)\cdot(1-2v)}{1-v}.$$

Following information is given for the 42CrMo4 steel specimen:

Table 7: Properties of the 42CrMo4 steel specimen [Richter, 2010].

Property and units	**Symbol**	**Value**
Young's modulus (10^9 N·m^{-2})	E	212
Poisson's ratio	ν	0.285
Density (kg m^{-3})	ρ	7834

To calculate the Young's modulus, the longitudinal sound velocity c_l needs to be known. According to the pulse-echo method, this is measured in transmission with two probes on each surface.

A thin gel layer is created on the respective surfaces. The probes are pressed lightly on the centre of the surfaces. Because sound velocity is measured in transmission, only the half of the distance of the specimen is measured. According equation (20), we then gain following relationship for the shown sound velocity c_x of the specimen [Schmidt-Döhl, 2014]:

$$c_x = c \cdot \frac{d}{2 \cdot d_x} \tag{21}$$

The length d_x is also shown at the screen. The parameter c is the actual sound velocity and d the actual length of the specimen, which can be read off the display scale or by the indication of the back wall echo position. The sound velocity c_x is read off the display, by adjusting the sound velocity c, in V-SCHALL, as long as

$$d = 2 \cdot d_x = 22.5\ mm \tag{22}$$

For an ideal view of the scale and the indication of the back wall echo, the parameter A-ANFANG is set, so that the aperture is at the same position as the back wall echo [Schmidt-

Döhl, 2014], and the parameters A-SCHWEL and dB in a way, that the echo can preferably be seen on the whole display. The value for c_x and consequently c is 5989 $m \cdot s^{-1}$.

Now, with the ascertained value for c and with equation (19) the Young's modulus can be determined:

$$E = 7834 \frac{kg}{m^3} \cdot \left(5989 \frac{m}{s}\right)^2 \cdot \frac{(1 + 0.285) \cdot (1 - 2 \cdot 0.285)}{1 - 0.285} = 217.15 \cdot 10^9 \frac{N}{m^2}$$

The deviation from the literature value [Richter, 2010] is 2.4%, which may result from inaccuracies in the measurement. One reason may be a deviation of the parameters from the values from literature. A precisely datasheet for the specimen was not available. Nonetheless, this deviation is in a tolerable range, which permits testing this measurement method on homogeneous isotropic ice Ih specimens to measure their Young's moduli.

6 Measurement of the Young’s modulus of ice

Until here, the fundamental knowledge was conveyed. Many authors have measured the Young’s modulus of ice using ultrasonic techniques. At the beginning, a state of the art will be presented. Then, the experimental preparations and the procedure itself will be explained.

6.1 State of the art

According Nanthikesan and Sunder (1994), there are three types of experimental techniques for determining the moduli of ice: the static methods, the dynamic methods and the sonic and ultrasonic methods. Most measurements until 1940 were made using static techniques applied to polycrystalline samples, which include tensile, bending and torsion tests (e.g. Hess, 1940 [Nanthikesan and Sunder, 1994]). A few dynamic measurements were carried out using polycrystalline samples in which the natural frequency of the characteristic mode of vibration of a small sample was observed (e.g. Ewing et al., 1934), but the results were quite imprecise [Gammon et al., 1983].

Northwood discovered in 1947 that it is possible to deduce the Young's modulus and the Poisson's ratio by measuring the velocity of various types of elastic waves in a solid. With sonic and ultrasonic methods, he determined experimentally the velocity of the wave to obtain the related elastic constants. By resonance in a rod, the longitudinal, extensional and Rayleigh wave velocities were measured in ice. The value obtained for the Young's modulus was $9.8 \cdot 10^9$ Nm^{-2} and for the Poisson's ratio was 0.335.

In 1948, a theoretical investigation of the elastic properties of ice single crystals was made by Penny using a simplified model of the ice crystal. This investigation led to a deduction of certain relations among the elastic constants. In 1952, Jona and Sherrer determined experimentally these constants from the optical diffraction patterns of crystals vibrating at high frequency. In 1956, Green and Mackinnon determined the elastic constants of an ice single crystal by a dynamical method, namely the measurement of the ultrasonic velocities of longitudinal and transversal waves along the c-axis of the crystal. For the growth of the ice crystals, constricted glass tubes full of distilled water were carefully suspended in a large tank. Their specimens were cylindrical ice crystals, 15 to 20 cm long and 2.25 cm in diameter, air free and clear as glass, where the orientation of the c-axis was known. The direct acoustic transit time through the specimens was measured. Two elastic constants were determined by solving a determinantal equation relating the elastic constants, the density, the sound velocity to the direction of travel of the sound wave through the crystal. For the remaining constants

the theory of Penny was applied. The values of the moduli of Penny (1948), Jona and Sherrer (1952) and Green and Mackinnon (1956) were quite similar. For the different direction of the axis the values vary between $3.26 \cdot 10^9$ Nm^{-2} and $16.2 \cdot 10^9$ Nm^{-2}. [Green and Mackinnon, 1956].

In 1964, Brockamp and Querfurth used a unit of Krautkrämer and applied the transit-time method to measure the sound velocities of the longitudinal and the transversal waves in plate likely lake ice specimens. Their measurements showed a temperature dependence of the longitudinal and the transversal wave and a transversal elastic anisotropy of the lake ice. From the velocities, they evaluated the elastic constants of hexagonal ice.

Proctor (1966) measured the sound velocities of single ice crystals at low-temperatures. He did not find any changes of the moduli at lower temperatures. A modified single-ended pulse technique was applied. His values for the moduli are in a range between $16.7 \cdot 10^9$ $N \cdot m^{-2}$ and $17.9 \cdot 10^9$ $N \cdot m^{-2}$.

The results of Dantl (1968) are considered as one of the most complete and the first of their kind. They are cited in recent works as well (e.g. Schulson and Duval, 2009). The velocity of sound has been measured using two different supersonic pulse methods; a transit-time method and a double impulse interference method. The specimens were grown strict after the gradient method, so the orientation of the c-axis can be determined exactly. With the help of the theory of Penny (1948) and the values of the longitudinal and transversal sound velocities, the complete set of the five elastic moduli had been determined.

The values measured by Gammon et al. (1982, 1983), are the most reliable to date [Schulson and Duval, 2009]. By using the technique of Brillouin spectroscopy, the dynamic elastic moduli of local homogeneous regions in ice samples, representing four different environments of formation, have been determined. The specimens included artificial ice, frozen from distilled water, clear monocrystalline glacial ice, bubbly lake ice and sea ice. He found, that the microscopic elastic properties of homogeneous monocrystalline ice do not to vary significantly with sample age, with impurities present at the time of freezing or with crystal quality. The values measured in their experiments, both for single crystal ice and for polycrystalline ice were taken as reference values in the present work.

In the technique of Brillouin spectroscopy (Figure 17) light from the hypersonic waves is scattered. With the Brillouin equation, which links acoustic propagation velocities to the

density and elastic moduli of a solid medium, the hypersonic velocities are obtained then [Gammon et al., 1983]. This technique was used by Gagnon et al. (1988) too. They measured the elastic constants of single ice crystals under loads of up to 10 kbar.

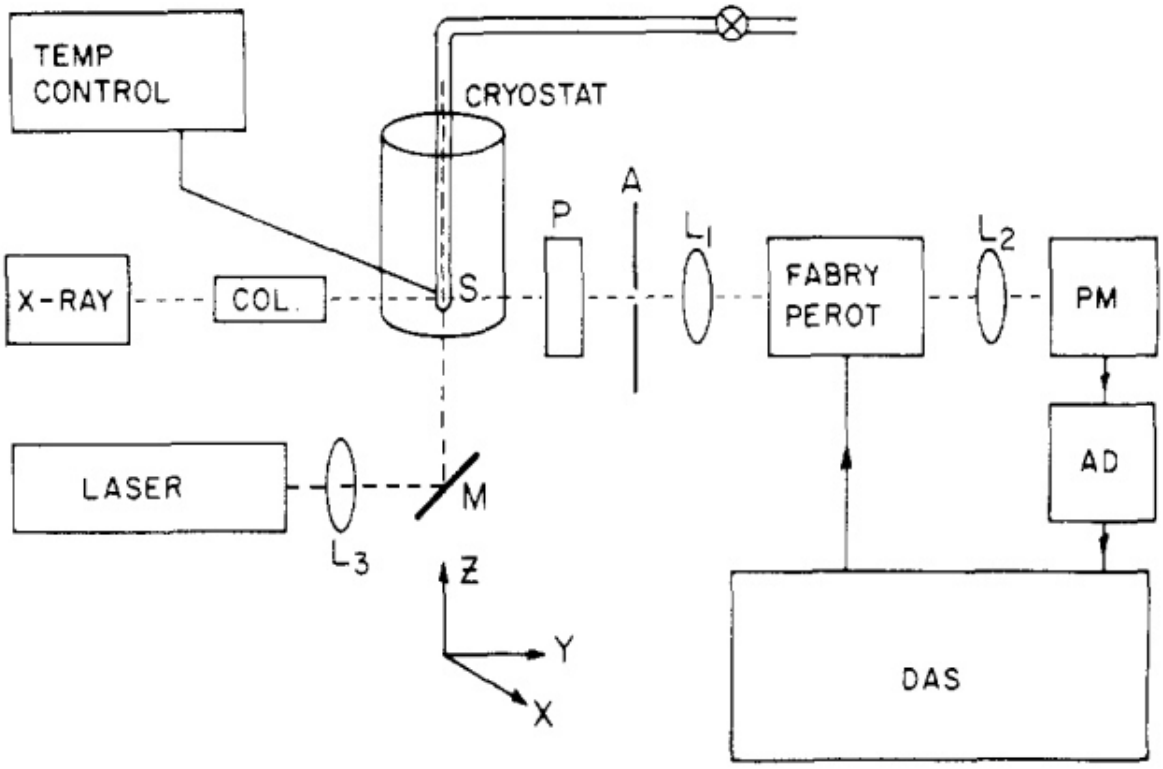

Figure 17: Brillouin scattering setup: S, sample cell; P, Polaroid X-ray camera; A, aperture and spatial filter; M, mirrors; L, lenses; PM, photomultiplier; AD, amplifier discriminator; DAS, data acquisition and stabilization system. [Gammon et al., 1982]

In 2008, Vogt et al. measured the sound velocity in bubble-free ice, using a linear array of six piezo ceramic lead zirconium titanate receivers. The array was deployed in a water tank, which was cooled down to −20 °C. The freezing process was performed inside a cooling container. Bubble-free ice was obtained using a freeze control unit, which filters and degases the water during the freezing process. The longitudinal and the transversal sound velocities were measured at temperatures between 0 and −20 °C.

With the help of several ultrasonic techniques (section 4.2), J. Krautkrämer and H. Krautkrämer (1990) have measured the Young's modulus and other material properties, like the Poisson's ratio and the shear modulus for many other materials than ice, as for instance

steel. Some units they constructed are used not only in laboratories, but also in the industry. In the present work, for the first time, the impulse-echo method after J. Krautkrämer and H. Krautkrämer (1990) is applied and tested for polycrystalline ice.

6.2 Experimental setup and test preparation

For the present experiments, first the ice specimens were prepared. In this section, the production of the ice specimens and their properties are presented. Further, the need of a bracket and the bracket itself will be explained. Further images from the experiments are shown in the appendix.

6.2.1 Production of ice specimen

The specimens are produced from leftover ice pieces, which broke off during other ice tests, performed in laboratories of the Institute for Ship Structural Design and Analysis of Hamburg University, with larger ice specimens. For the ice, only few information are known: the specimens are made of commercial crushed-ice and distilled water. The crushed-ice is mixed with the water and the alloy is then frozen at -10°C. The ice is composed of randomly oriented grains and is therefore elastically isotropic (see section 3.2). The grain size is nearly 2.5 mm. The pore content is not analysed yet.

The specimens were prepared and stored in a refrigeration container, where they also were sawed in totally nine cuboids with different metrics (Figure 18). For later analysis, one specimen (S02) is compressed slow and slightly in a vice, until a crack forms (Figure 19). The specimen with crack is then defined as SC02. As assumed in section 3.3, the crack arises parallel to the direction of the applied compression stress [Schulson and Duval, 2009]. One inhomogeneous specimen (SI, Figure 20) with an optical distinct boundary between crushed ice and distilled water was kept for further measurements.

Figure 18: Cuboid ice specimen

Figure 19: Crack can be seen through the surface of the cracked specimen

Figure 20: Inhomogeneous specimen SI

6.2.2 Ascertaining the properties of the specimens

All specimens are cuboid. The geometrical dimensions are defined in Figure 21. First of all, a cubical trial specimen ST with an edge *length l* = 45 mm was manufactured. From the results of the measurements of ST, the other specimens were produced. The requirement was that specimen with different length l and random *breadth b* and random *height h* were prepared. But for reasons of operability and ergonomics, b and h were in the range of 50 mm to 155 mm. The values for the lengths of the different specimens are given in Table 8.

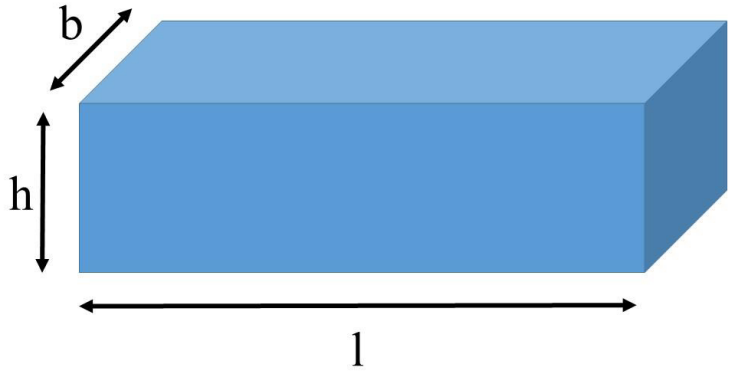

Figure 21: Geometrical properties of cuboid specimen

Table 8: Lengths of the different specimen.

Name of specimen	**Length l (mm)**
ST	45
S01	50
S02	60
S03	70
S04	100
S05	135
S06	154.4
SC02	60
SI	140.5

Next, the *density* ρ was determined. Therefor the *mass m* was weighed at room temperature with a balance and the *volume V* was calculated by the product of $V = h \cdot b \cdot l$. The breadth b and height h were measured with a caliper. Table 9 lists the values for the density of the specimens. The density was calculated with the relation

$$\rho = \frac{m}{V}. \tag{23}$$

Table 9: Density of the specimens.

Specimen	**Density (kg·m^{-3})**
ST	908.64
S01	924.52
S02	930.11
S03	916.28
S04	928.26
S05	913.72
S06	900.96
SC02	936.37
SI	897.45

Because the respective values of the densities vary, it is advantageous to calculate the average of the densities of the specimens. For further calculations, one consistent value will be used for the density. The average of the densities, except the density of SI, amounts to ρ = *920.41 kg·m^{-3}*, with which subsequent calibrations will be conducted. In literature, the value for the density of ice is also stated in this range [Bader, 1964; Gammon et al., 1983; Schulson and Duval, 2009].

The Young's modulus can be determined by equation (15) with the transversal wave of the ice specimens. The transversal wave can be measured with an angel-beam probe [Berke, 1996]. Because an angel-beam probe was not available, the Young's modulus will be determined by equation (19), with the Poisson's ratio. Values from literature state the Poisson's ratio in a wide range, for example:

Table 10: Poisson's ratio of ice by different authors

Author	**Poisson's ratio ν (kg·m^{-3})**
Weeks and Assur (1967)	0.25 – 0.38

Gammon et al. (1982; 1983)	0.325
Gagnon et al. (1988)	0.324
Nanthikesan and Sundar (1994)	0.325 – 0.329
Schulson and Duval (2009)	0.224-0.415

The most current value for the Poisson's ratio of isotropic polycrystalline ice Ih is given by Schulson and Duval (2009) as $\nu = 0.325$, with which subsequent calibrations will be conducted.

6.2.3 Bracket

After measurements with specimen ST (explained in section 6.3), some challenges occur operating the unit. While the probes were connected to the specimen, it was difficult to simultaneously vary the value of the sound velocity c in V-SCHALL, and record the results. Moreover, the back wall echo depends very much on the pressure of the probes on the specimen (see chapter 6.3). Also, due to reasons of operability and ergonomics, a bracket was constructed. It keeps the probes in fix positions, exerts sufficient pressure on the probes and is able, depending on the size of the specimen, to adjust the distance between the probes (Figure 22). The technical drawing of the bracket was created with Autodesk Inventor 2017. The bracket was constructed in the laboratories of the Institute for Ship Structural Design and Analysis of Hamburg University. The material of the underlay and the bracket is wood. The track and the accompanying carriage are purchased parts made from steel. The probes were placed in the brackets and positioned from above by a mounting head with the same shape as the probes. The mounting head is adequately screwed down to the body of the bracket with two screws. The specimen is then connected to the probes in the bracket. Possibly a wooden block is used to increase the position of the specimen, so that it is on the same height as the probes. The probe in the movable bracket is then moved to the specimen and pressed sufficient on it (Figure 23). The carriage in the track has an adequate self-locking effect, so that it can be moved unproblematically in the track, but sufficient pressure is applied on the specimen by the probes. Thus, the movable bracket has an appropriate self-locking effect. More images of the bracket, and the technical drawings are to find in the appendix. The ipt.- and dwg-files of the bracket are available on the data medium.

Figure 22: Bracket

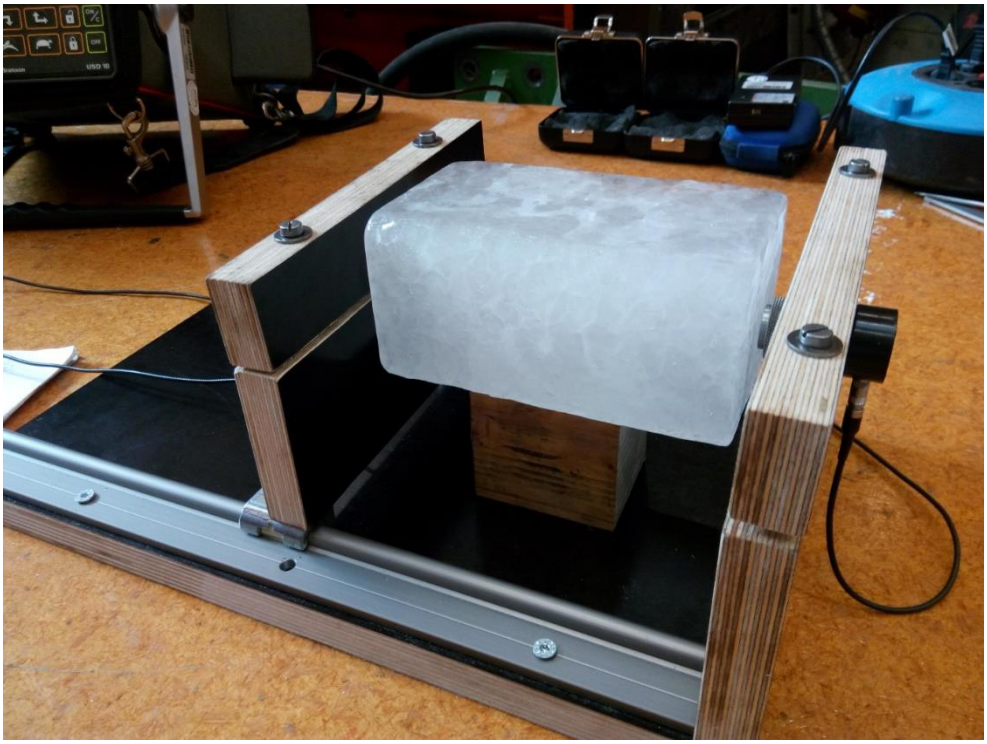

Figure 23: Test setup

6.3 Experimental procedure

It is not allowed to use the unit in the cooling container, hence all measurements were carried out at room temperature. If a specimen was not in use, it was stored in the refrigeration container.

Before other specimens were produced, experiments were carried out with the test specimen ST. The specimen was placed on a wooden table and the surface to be measured was lubricated with a thin layer of gel and then connected to the probes. The geometrical dimensions were known, thus with equation (21), the longitudinal sound velocity c_x can be displayed through adjusting the sound velocity c, in V-SCHALL, as long as $d = 2 \cdot d_x = 22.5\,\text{mm}$. Because of a strong basis line noise, the gain dB have to be increased, to differentiate the back wall echo from the interfering signal. The amplitude is not visible completely anymore. Though, with the zoom function of the unit, the horizontal position is still displayed on the screen. Therefor the parameter A-ANFANG is set, so that the aperture is at the same position as the back wall echo, or the geometrical length of the specimen. In addition, the parameter A-BREITE is set, so that the back wall echo is also indicated in a certain deviation from the geometrical length, so the sound velocity can be adjusted depending on the deviation. With this, the sound velocity of the ice specimen is set to $c_x = 3970\ \text{m s}^{-1}$ and the Young's modulus of the homogenous polycrystalline ice Ih can be determined by equation (19) with the Poisson's ratio of $\nu = 0.325$ [Schulson and Duval, 2009] and the average density $\rho = 920.41\ \text{kg m}^{-3}$:

$$E = 920.41 \frac{kg}{m^3} \cdot \left(3970 \frac{m}{s}\right)^2 \cdot \frac{(1 + 0.325) \cdot (1 - 2 \cdot 0.325)}{1 - 0.325} = 9.962 \cdot 10^9 \frac{N}{m^2} \tag{24}$$

Next, the horizontal and the vertical positions of the probes were changed on the surface. The value of the shown sound velocity c_x, and therefore the value of the Young's modulus, did not change. These values also remain constant when the probes were connected to the respective other surfaces of the specimen ST. These results confirm the elastic isotropy in ice, as mentioned in chapter 3.

The most accurate value to date for the Young's modulus of isotropic polycrystalline ice Ih was measured by Gammon et al. (1983), $E = 9.332\ 10^9\ \text{N}\cdot\text{m}^{-2}$. The deviation from this value amounts to 6.3%. This allows to proceed with measurements on other ice specimens.

Because the measurements were carried out at room temperature, meltwater formed on the surface of the specimen. The layer of gel does not remain on the surface. As mentioned in section 4.1, water can be used for the coupling media. Because here the water is produced

continuously, it is a convenient coupling media and will be used in all subsequent experiments.

With ongoing time, the probes have to be connected continuously stronger to the specimen, to obtain a readable signal of the back wall echo. After approximately 7 minutes, in the repetition of the measurements with specimen ST, the signal of the back wall echo was very weak and the noise very strong. The first assumption was that the probes were quenched after first measurements, because the probes became very cold. Therefore, after 15 minutes and the storage of the specimen in the refrigerating container in the repeated measurement, the signal of the back wall echo was stronger, but still very weak. The assumption for this was that at cold temperatures the probes connect very poor. However, this was not the reason. After the surface was cleaned from the meltwater, this problem did not emerge again. The amount of meltwater was too large. With poor and in this case too thick layer of coupling media, the signal of the back wall echo is diluted [Tietz, 1974]. Moreover, these probes can be used, according the manufacturer, at temperatures of -10°C. So, the coldness' effect on the probes was not the problem here.

Because the reason of the poor signal was known, the aim was to keep an adequate amount of meltwater on the surface of the specimen. Cleaning the surface after short time periods was strenuous. If required, an appropriate pressure was applied on the probes, so that in cases of larger amounts of meltwater, sufficient contact is ensured for a readable signal of the back wall echo. The reason, why it was not possible to detect the back wall echo again after 15 minutes, was that ice melts with ongoing time and the layer of the meltwater becomes too thick. In the following measurements, where the bracket, described in section 6.2.3, was used, problems like too strong noise, too low pressure or other ergonomic problems did not occur again.

The measurements with S01-S06 and SC02 were similar to the measurements with specimen ST. The differences were, no gel was used as coupling media and the probes were chucked in the brackets. The specimen was put on a block of wood and one surface was connected to the fix probe. The flexible bracket was pressed onto to the specimen. With this, the other probe was connected with an sufficient pressure to the other surface, too (Figure 24; Figure 25).

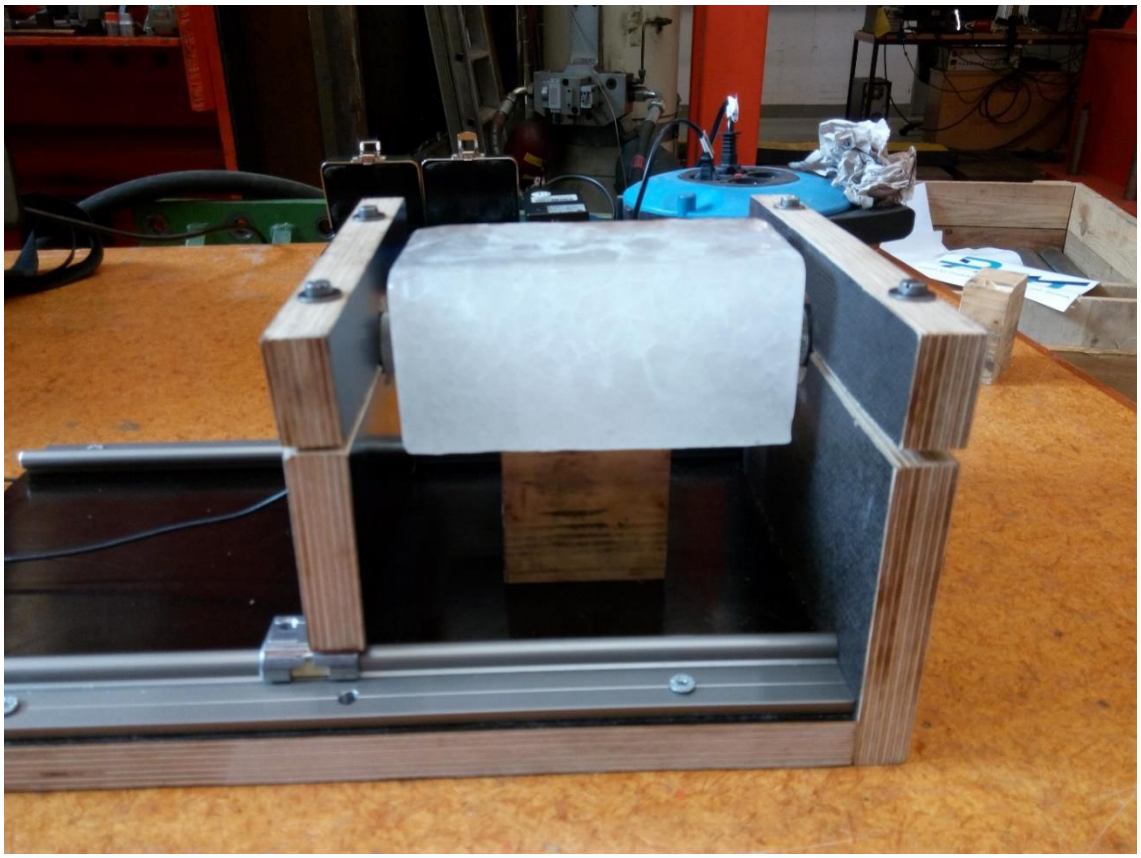

Figure 24: Specimen between the probes

Figure 25: Contact surface

Next, the cracked specimen SC02 was measured. SC02 was compressed parallel to l (Figure 21) and a crack was formed. The definition of this specimen after crack is SC02. Unlike in the measurements before, here the sound velocity c was measured parallel to l, b and h, because along every axis the sound velocity varies in SC02. Lastly, the sound velocity of the remaining inhomogeneous specimen SI was measured, too. Because of the optical distinct boundary between the crushed ice and the distilled water, the sound velocity was measured individually for the part with crushed ice and once for the part with distilled water. All values measured for the sound velocities and from that calculated Young's moduli are given in chapter 7. For all specimens, these measurements were repeated after 60 minutes, after the specimens were stored again in the refrigerated container. Almost same values were gained. The minimal changes are not notable, but explained in chapter 7.

7 Results and discussion

In the experiments, the sound velocity of the respective specimens was measured. From this, the Young's modulus was calculated, as explained in the previous chapter. The numeric values of these parameters are given in Table 11:

Table 11: Sound velocity and the Young's modulus of the specimens

Specimen			**Sound velocity c ($m \cdot s^{-1}$)**	**Young's modulus E (10^9 $N \cdot m^{-2}$)**
S01			3830	9.272
S02			3890	9.565
S03			3950	9.862
S04			3930	9.762
S05			3840	9.320
S06			3860-3880	9.418-9.516
ST			3820	9.224
SC02, measured parallel to	l		3830-3860	9.272-9.418
	b		3440	7.480
	h		3770	8.984
SI	crushed ice	l	3920-3930	9.713-9.762
		b	3920-3930	9.713-9.762
	distilled water	l	3800-3810	9.127-9.175
		b	3800-3810	9.127-9.175
	h		3860-3870	9.467

For specimens S01-S06 and SC02, the values of the sound velocity vary between 3820 and 3950 m s^{-1}. According equation (19), the Young's modulus depends quadratically from the sound velocity. Thus, the values of the Young's modulus of the specimens vary. Nonetheless the range of the values of the Young's moduli are approximately in the same range as the

reference value of E = 9.332 10^9 $N \cdot m^{-2}$ (Gammon et al., 1983). The maximum deviation from this value amounts to 9.5%. In Table 12 some values for the longitudinal sound velocity in ice are given. The measured values for the sound velocity in the specimens are approximately in the same range. Here, it is important to annotate, that not all authors have made specification about the preparation and composition of their ice specimens. The sound velocity and the Young's modulus depend strongly on parameters during the production of the ice (see chapter 3). This may be the reason for the deviation from the values, measured in the present experiment.

Table 12: Values for the longitudinal sound velocity in ice by different authors

Author	**Sound velocity ($m \cdot s^{-1}$)**
Tietz (1969)	3980
Kuppermann and Reimann (1980)	3950
Sayers (1982)	2800-3900
Gammon et al.(1983)	3892-4040

The respective measured values of the cracked specimen SC02 deviate strongly from the measured value before the crack occur (S02). The sound velocity parallel to the axis l, where the compressive stress was applied, has a minor decrease to the sound velocity of the crack-free specimen S02. Perpendicular to the strained axis the respective values of the sound velocity are decreased strongly. As said in chapter 3.3, the stiffness of the specimen is reduced after the crack. SC02 was the only specimen, which was not elastically isotropic. As mentioned in chapter 3.3, the three-dimensional isotropy is degraded, when the specimen is compressed to the extent that along the direction of maximum compressive stress an axis-symmetric array of cracks develops [Schulson and Duval, 2009]. These measurements support this assumption. However, they do not confirm completely, that the elastic behaviour of cracked ice may be described in a manner similar to that used to describe the behaviour of Ih single crystals [Schulson and Duval, 2009]. Therefore, further measurements along different axis, as mentioned in section 3.1, are necessary.

The elastically isotropy of polycrystalline ice, mentioned in section 3.2 is confirmed here. Also, the other assumptions regarding the coupling media, the pressure on the probes and

assumed from this some other statements, during the measurement of specimen ST, were confirmed for specimen S01-S06 and SC02.

Other conclusions for the ultrasonic measurement of ice can be gained from the results of the inappropriate specimen SI. In specimen SI, an optical distinct boundary between crushed ice and distilled water was visible. The respective values for the different parts of specimen SI, given in Table 11, are constant along the l and b axis. Parallel to the h-axis, the value is the average of the respective sound velocities of the crushed ice part and distilled water part. From that, it is known that the respective parts of the specimen SI are isotropic and the sound velocity through the whole specimen is the average of the respective sound velocities. This may depend on the respective portion of the blend. However, this is only a supposition, because there is no reference value for such a blend. For an exact statement more experiments are necessary with more specimens existing of composites. Nevertheless, it is possible to measure the sound velocity and then calibrate the Young's modulus for ice specimens with an unknown composition and manufacturing. If in future exact reference values for the sound velocity of different manufactured ice specimens are known, it is possible to exactly classify the specimen. As the results show, it is possible for individual homogeneous specimens. So, the specimen SI was not inappropriate, because many new knowledges was gained due to the inhomogeneous composition of this specimen.

In the repeated measurements, for some specimens the value of the sound velocity varied. This fluctuation is also given in Table 11. Because the specimen started melting, they deformed easier. When the probes then were pressed on the surface of the specimen, little imprints aroused on it. With this, the surface was not plane anymore. However, this is required for the ultrasonic method applied in these experiments. Because of the deformation, it was possible, through pressing the probes stronger on the specimen surface, to deform it plane again. The sound velocity measured then has the given deviation perpendicular to the surface. This may result from the fact, that the surfaces are not exactly plane anymore. If the surfaces are not plane, the sent wave will not be reflected back completely (Figure 12). The transversal part of the wave is not measured then, and this will lead to a measured decrease of the Young's modulus. Also, the fact that the beam may be refracted at the single crystals of the ice, leads again to a lesser reflection of the beam. And this inaccuracy should not be neglegated. The values of the Young's modulus are approximately in tune with values from literature. But the exact value of the Young's modulus for a random specimen will not be known, until the reflection at the single crystals of ice is not completely researched.

There is no provision for the exact pressure of the probes on the specimen surfaces. This was, despite of the bracket, a disadvantage. Depending from the variable pressure, the strength of the signal and thus the vertical position of the peak of the back wall echo changes. The higher the pressure, the higher the peak. The horizontal position of the peak however, does not change. Consequently, the sound velocity remains the same. But reading the unit display, ergonomic difficulties can occur, because the vertical position of the zoom function must be changed, else the unit will show the position of another point of the signal than the peak. The fluctuation of the signal during the variation is reasoned due to the coupling of the probes. The higher the pressure on the probes the smaller is the vacuum between probe and surface.

The peak of the signal depends also on the length of the specimen. In this experiment, it was apparent that the amplitude was very high for short specimens, for instance ST. For longer specimens the amplitude becomes weaker. The limit for a minimum and a maximum length is unknown, especially for ice. Nevertheless, it would be possible to differ an extreme weakened amplitude from noises. With the right settings of the zoom function, this would not be a great challenge.

As mentioned above, the specimens start melting during the measurements, because the experiments were carried out at room temperature. Schulson and Duval (2009) measured a pressure-induced reduction of the melting point of 0.074°C/MPa. The pressure induced by the probes was not that high, but it has also an influence on the melting point. On one side, the meltwater was an advantage, because the meltwater was used as coupling media. On the other side, the melting water impeded the experiments. For one thing, too much meltwater impaired the quality of the back wall echo signal, secondly the specimens' length changed. The developed melt water was wiped and with this, the specimen becomes smaller. Until approximately seven minutes after the specimen was extracted from the refrigerated container, the vertical position of the peak does not change. Here the melt water may be adequate, but after 15 minutes the signal was weakened very strong, so that the back wall echo could not be seen anymore. The developed melt water then had to be wiped. The melting became higher with ongoing time. The relation between the ice temperature and the time is given in equation (12). However, the influence of the temperature and time was not taken into account in these experiments. How the signal of the back wall echo behaves, if the experiments would be conducted in the refrigerated container, may be part of future experiments.

Also, many mathematical and mechanical inaccuracies appeared. For the calculation, the Poisson's ratio is taken from literature, although it varies for different manufactured ice specimens. The actual value for the specimens, used in this project, is not examined yet. According Hüth (1977), the Poisson's ratio is subjected natural principle of orders. Its value is not only in the range of 0.25 and 0.5, but it has a functional subordination from the Young's modulus and from this, a matter systematology can be observed. For an independent and exact measurement of the Young's modulus, the Poisson's ratio and the density should be chosen and defined independently. If only values from literature are used, the actual values of the elastic properties for an ice specimen will never be obtained.

The density, as shown in the previous chapter, varies for each specimen. This may be reasoned due to the fact that the specimens are broken off leftover from another larger specimen. The larger specimen was already compressed and force was applied, therefore the mechanical properties should have been changed, in comparison to an unloaded specimen. In the present work, the Young's modulus was calculated with a theoretical value, too. For the density the average of all densities was chosen. In addition, the shown value for the sound velocity may be not completely accurate. For instance, the sound velocity was displayed not more precise than in intervals of 10 (see Table 11). In modern units, such problems will not occur. All these impurities play a significant role in the calculation of the Young's modulus. If the respective parameters vary, the value of the Young's modulus changes according to them.

8 Conclusion and outlook

In the present work, the Young's moduli of three different types of ice specimen were determined. One inhomogeneous specimen with an optical distinct boundary between crushed ice and distilled water, one cracked and seven crack-free polycrystalline homogenous ice specimens were examined.

According the impulse-echo method, the longitudinal sound velocities were measured in two applications in all specimens and from this, the Young's moduli were calculated. Although an overall scatter was recorded, the individual values for the respective specimens remain constant. The range of the measured values of the sound velocity and the Young's modulus are approximately in the same range as values in literature, whereby different authors have measured very different values for the velocities and the mechanical properties.

It was not clear, whether the scatter is reasoned due to inaccuracies in the measurement or due to incorrect specimens. But after the discussion and analysis of the results, it became clear that some important factors have been overlooked and should be taken in account in future experiments.

The specimens were too vague. Firstly, they were leftover from another already stressed specimen. Secondly, they were all composited differently, which can be seen from the fact that the densities of all specimen varied strongly.

The dependence of the temperature was neglected, though elastic properties of ice depend from it. The experiments were conducted at room temperatures, but all comparative values were measured at degrees below zero and could therefore not be properly in line with the present values. How the values changes, when the values are obtained in the refrigerated container, can be measured in future experiments.

The Young's modulus was calculated with theoretical values, like the Poisson's ratio, which was taken from literature, and the average of the densities. The result from this cannot be the actual value for the Young's modulus, but rather a rough estimation for it. For the actual value, the calculation should be conducted with the respective density and the individual Poisson's ratio, which have to be measured independently. As in previous experiments, at least two properties have to be measured independently to derive the other properties from this.

This problem can be solved with an angle beam. With this, the transversal sound velocity can be measured too. Then it is even possible to calculate the respective Poisson's ratio of different specimens. During the experiments no information about a potential reflection of the beam at single ice crystals was obtained. With an angle beam a qualitative and quantitative answer for this may be received.

Nevertheless, many statements were in line with previous works and new knowledge was gained. The elastic isotropy of polycrystalline ice specimens was confirmed. During measurements on the complete surfaces, on two respective plan parallel sides, the sound velocity remained constant. An almost identical value was documented for the other surfaces.

In the inhomogeneous specimen, the respective constant values were measured for the sound velocities of the longitudinal waves in the respective parts constant for two directions. The value in the crushed ice part was in the same range as the sound velocities of the other polycrystalline ice specimens. The sound velocity through both parts was the average of the respective sound velocities. This may be reasoned to a consistent proportional of both parts. However, it is necessary that this suppose has to be investigated in more experiments with such composites.

The anisotropy of ice after crack, presumed by Schulson and Duval (2009) was confirmed for the cracked specimen. The experimental results of the cracked specimen gave varying values lower than those deduced for the crack-free specimen. This is also in line with conclusions by Schulson and Duval (2009). Nonetheless, more specimens for homogenous and cracked samples are required to obtain accurate results. With another ultrasonic method, namely the sound emissions analysis, it is also possible to detect and analyse cracks and other defects as pores and cavities. In further work, cracks may be examined with this method.

Because of the meltwater, formed on the surfaces, no gel as coupling media was needed. With ongoing time, the melting increased, thus signal became weaker, because it was not reflected properly anymore. Because of the melting and a better ergonomic, a bracket was constructed and used.

All in all, very valuable conclusions can be taken from this work. Many results were in line with literature, but some important questions still remain unsolved.

At the present state, the applied technique is applicable, to measure temporarily and roughly the longitudinal sound velocity in a homogenous polycrystalline ice specimen, detect

different types of ice with different composites and manufacturing, and to identify a change of elastic properties after crack.

For precise and proper results further experiments with unified grown specimens have to be conducted. An independent measurement of the transversal sound velocity is indispensable. Than it may also be possible to determine the other mechanical properties independently. Until then, conventional methods have to be applied to measure mechanical properties of polycrystalline ice.

On the basis of this knowledge, it may be possible to develop a simple, precise, time-saving and cost-saving technique in future, by which the Young's modulus can be measured and ice can be classified.

Bibliography

[Bader, 1964] Bader, H. (1964). Criteria for measurement of strain rates in deep bore holes in polar glaciers. Hanover, NH: U.S. Army Material Command, Cold Regions Research & Engineering Laboratory.

[Berke, 1996] Berke, M. (1996). Nondestructive material testing with ultrasonics: introduction to the basic principles. Krautkamer GmbH & Company.

[Bragg, 1922] Bragg, W. H. (1922). The significance of crystal structure. Journal of the Chemical Society, Transactions, 121, 2766-2787.

[Brockamp and Querfurth, 1964] Brockamp, B., & Querfurth, H. (1964). Untersuchungen über die Elastizitätskonstanten von See-und Kunsteis. Polarforschung, 34(1/2), 253-262.

[Dantl, 1968] Dantl, G. (1968). Die elastischen Moduln von Eis-Einkristallen. Zeitschrift für Physik B Condensed Matter, 7(5), 390-397.

[Durham and Stern, 2001] Durham, W. B., & Stern, L. A. (2001). Rheological properties of water ice—Applications to satellites of the outer planets. Annual Review of Earth and Planetary Sciences, 29(1), 295-330.

[Elvin, 1996] Elvin, A. A. (1996). Number of grains required to homogenize elastic properties of polycrystalline ice. Mechanics of materials, 22(1), 51-64.

[Ewing et al., 1934] Ewing, J. (1934). Neoplastic diseases. WB Saunders; London.

[Gammon et al., 1982] Gammon, P. H., Kiefte, H., & Clouter, M. J. (1982). Elastic constants of ice samples by Brillouin spectroscopy. The Journal of Physical Chemistry, 87(21), 4025-4029.

[Gammon et al., 1983] Gammon, P. H., Kiefte, H., Clouter, M. J., & Denner, W. W. (1983). Elastic Constants of Artificial and Natural Ice Samples by Brillouin Spectroscopy. Journal of Glaciology, 29(103), 433-460.

[Gagnon et al., 1988] Gagnon, R. E., Kiefte, H., Clouter, M. J., & Whalley, E. (1988). Pressure dependence of the elastic constants of ice Ih to 2.8 kbar by Brillouin spectroscopy. The Journal of chemical physics, 89(8), 4522-4528.

[Gold, 1958] Gold, L. W. (1958). Some observations on the dependence of strain on stress for ice. Canadian Journal of Physics, 36(10), 1265-1275.

[Green and Mackinnon, 1956] Green Jr, R. E., & Mackinnon, L. (1956). Determination of the elastic constants of ice single crystals by an ultrasonic pulse method. The Journal of the Acoustical Society of America, 28(6), 1292-1292.

[Hess, 1940] Hess, H., 1940. Z. Gletscherkd., 27: 1.

[Hobbs, 1974] Hobbs, P. V. (1974). Ice Physics, Oxford Classic Texts in the physical sciences. Oxford, UK: Oxford University Press.

[Häusler, 1989]. Häusler, F. U. (1989). Beitrag zur Ermittlung der Kräfte beim Eisbrechen unter besonderer Berücksichtigung der Anisotropie des Eises und seiner

Versagenseigenschaften unter mehrachsiger Beanspruchung. Schriftenreihe Schiffbau, Hamburg.

[Hutter, 1983] Hutter, K. (1983). Theoretical glaciology; material science of ice and the mechanics of glaciers and ice sheets, D. D. Reidel Publishing Co./Tokyo, Terra Scintific Publishing Co.

[Hüth, 1977] Hüth, R. (1977). Über die Elastizität der kristallinen Festkörper. Materials Science and Engineering, 29, 55-97. Netherlands.

[Jona and Sherrer, 1952] Green Jr, R. E., & Mackinnon, L. (1956). Determination of the elastic constants of ice single crystals by an ultrasonic pulse method. The Journal of the Acoustical Society of America, 28(6), 1292-1292.

[J. Krautkrämer and H. Krautkrämer, 1986] Krautkrämer, J., & Krautkrämer, H. Werkstoffprüfung mit Ultraschall, 5. Völlig überarbeitete Auflage. Berlin: Springerverlag, 1986. ISBN 3-540-15754-9.

[J. Krautkrämer and H. Krautkrämer, 1990] Krautkrämer, J., & Krautkrämer, H. (1990). Ultrasonic Testing of Materials, 4th fully revised Edition. New York: Springer-Verlag Berlin Heidelberg. ISBN 3-540-11733-4.

[Kupperman and Reimann, 1980] Kuppermann, D. S.; Reimann, H. J.: Ultrasonic NDE of cast stainless steel. NDT Intern. 20 145-152.

[Liu et al., 1995] Liu, S.-N.; Light, G. M.; Joshi, N. R.: Ultrasonic detection of stress-corrosion cracks in reactor pressure vessel and primary coolant system anchor studs (bolts). Mater. Eval. 45, 1413-1418.

[Morris, 2007] Morris, J.W.: A Survey of A Survey of Materials Science Materials Science I. Structure. Berkeley.

[Michel, 1978] Michel, B. (1978). Ice mechanics. Québec: Presses de l'universite Laval.

[Millner et al., 1987] Millner, R. (1987): Wissensspeicher Ultraschalltechnik. Leipzig: VEB Fachbuchverlag.

[Nanthikesan and Sunder, 1994] Nanthikesan, S., & Sunder, S. S. (1994). Anisotropic elasticity of polycrystalline ice Ih. Cold regions science and technology, 22(2), 149-169.

[Northwood, 1947] Northwood, T. D. (1947). Sonic determination of the elastic properties of ice. Canadian Journal of Research, 25(2), 88-95.

[Nye, 1992] Nye, J. F. (1992). Water veins and lenses in polycrystalline ice. Physics and chemistry of ice, 200-206.

[Penny, 1948] Penny, A. H. (1948, July). A theoretical determination of the elastic constants of ice. In Mathematical Proceedings of the Cambridge Philosophical Society (Vol. 44, No. 3, pp. 423-439). Cambridge University Press.

[Proctor, 1966] Proctor Jr, T. M. (1966). Low-Temperature Speed of Sound in Single-Crystal Ice. The Journal of the Acoustical Society of America, 39(5A), 972-977.

[Richter, 2010] Richter, F. (2010): The Physical Properties of Steels „The 100 Steels Programme" Part I: Tables and Figures. Mühlheim a.d. Ruhr.

[Schmidt-Döhl, 2014] Schmidt-Döhl, F. (2014): Qualitätsmanagment-Handbuch Arbeitsanweisung TUHH-B3-AA111-1. Bedienung des Ultraschallgerätes Krautkrämer USD10. Hamburg

[Schulson and Duval, 2009] Schulson, E.M., & Duval P. (2009). Creep and Fracture of Ice. Cambridge: Cambridge University Press.

[Schulson, 1999] Schulson, E. M. (1999). The structure and mechanical behavior of ice. JOM journal of the Minerals, Metals and Materials Society, 51(2), 21-27.1 (2) (1999), pp. 21-27.

[Tietz, 1969] Tietz, H. D. (1969): Ultraschall-Meßtechnik. VEB Verlag Technik Berlin.

[Tietz, 1974] Tietz, H. D. (1974): Ultraschall-Meßtechnik. Messtechnik, Berlin: VEB Verlag Technik Berlin.

[USD 10 Basic operation guide]. (n.d.). Retrieved November 1, 2017, from Krautkrämer Branson

[Vogt, 2008] Vogt, C., Laihem, K., & Wiebusch, C. (2008). Speed of sound in bubble-free ice. The Journal of the Acoustical Society of America, 124(6), 3613-3618.

[Weeks and Assur, 1967] Weeks, W. F., & Assur, A. (1967). The mechanical properties of sea ice (No. SCIENCE/ENGINEERING-2-C3). COLD REGIONS RESEARCH AND ENGINEERING LAB HANOVER NH.

Appendix

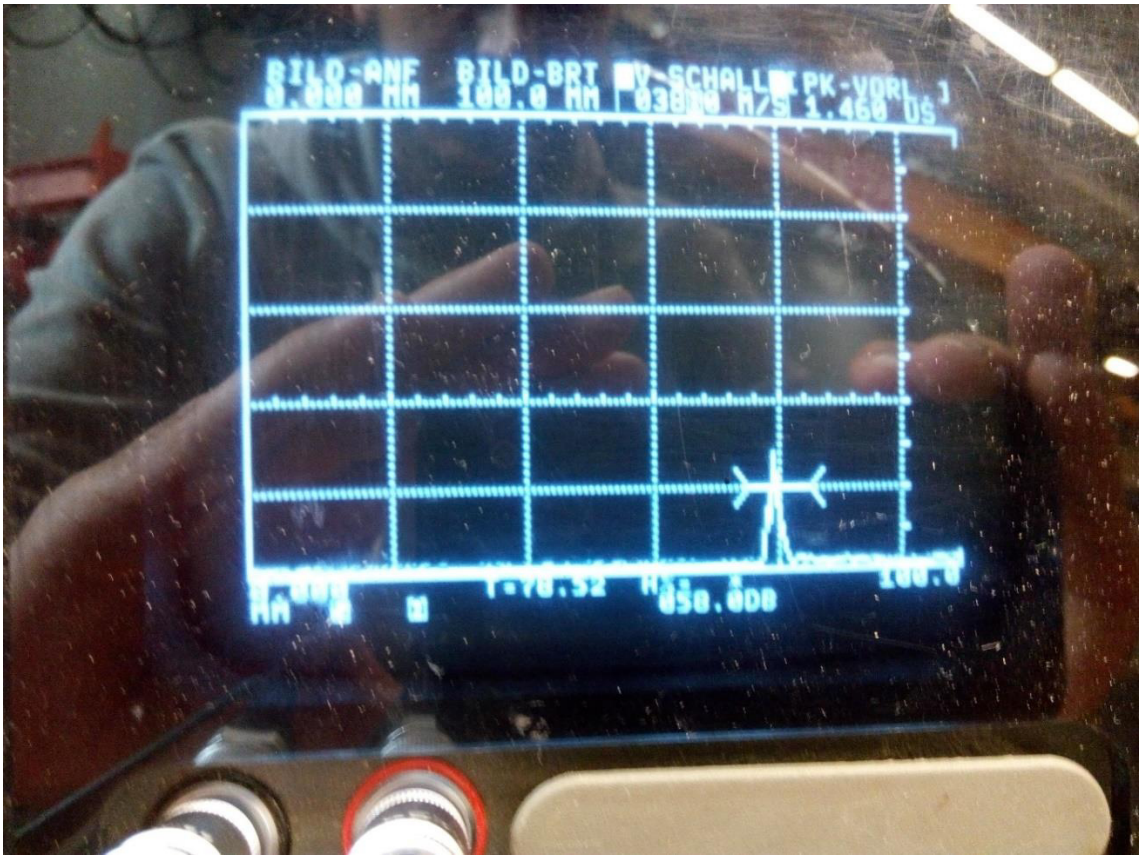

Figure 26: An indicated back wall echo at the length $T = 78.52$

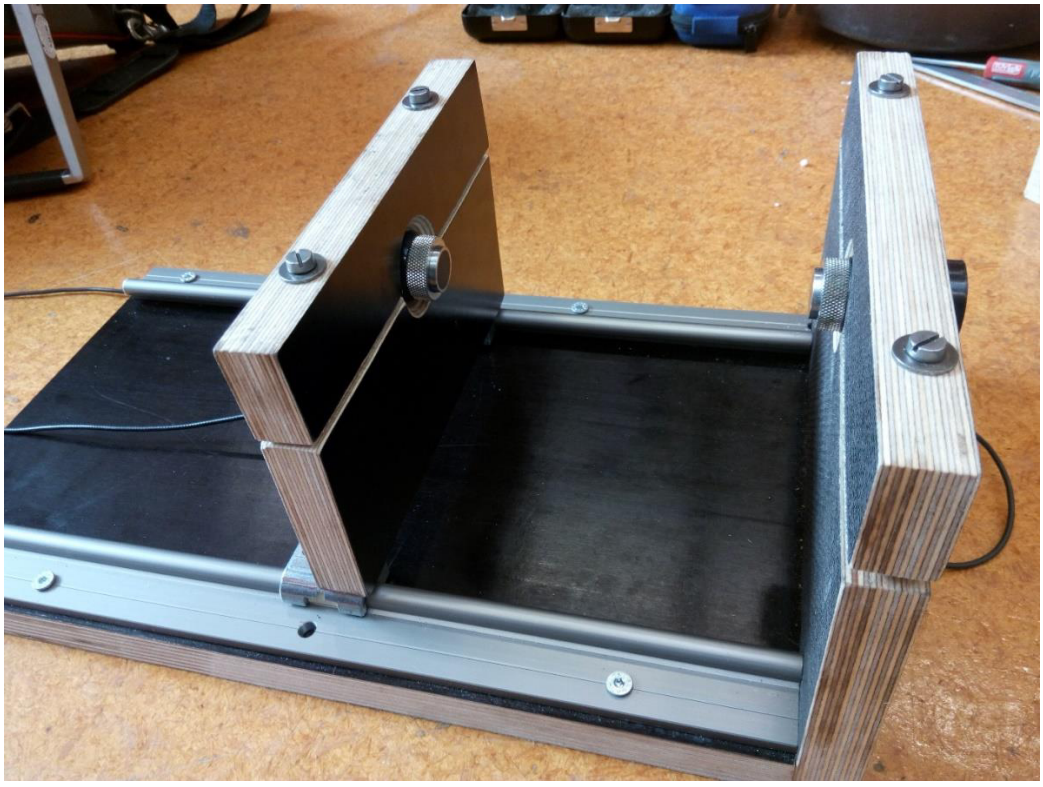

Figure 27: The probes are fixed in the brackets.

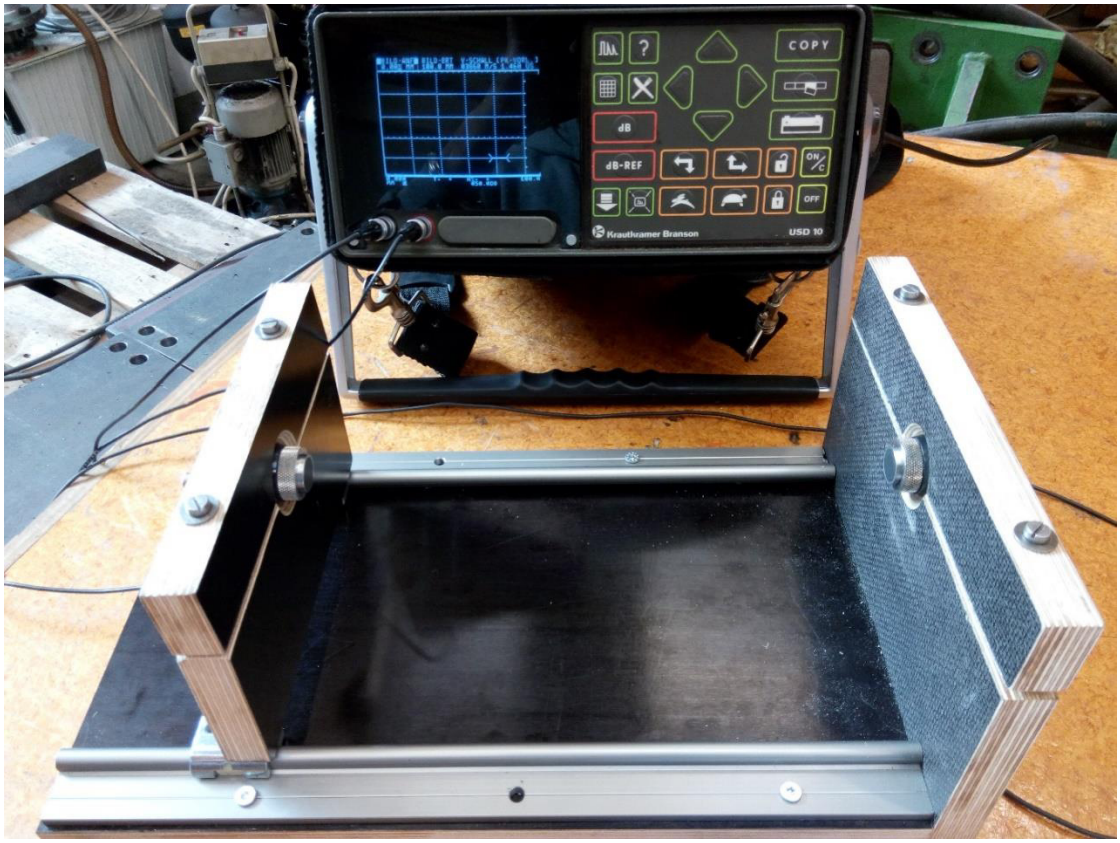

Figure 28: The probes in the bracket are connected to with the unit.

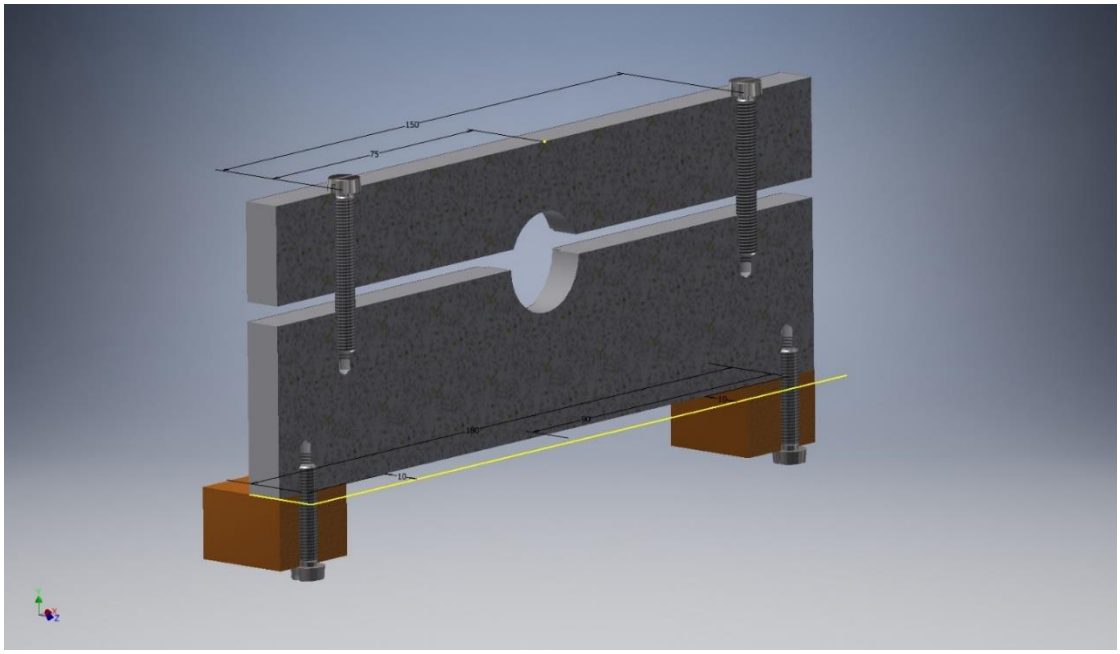

Figure 29: Screw joints in the bracket

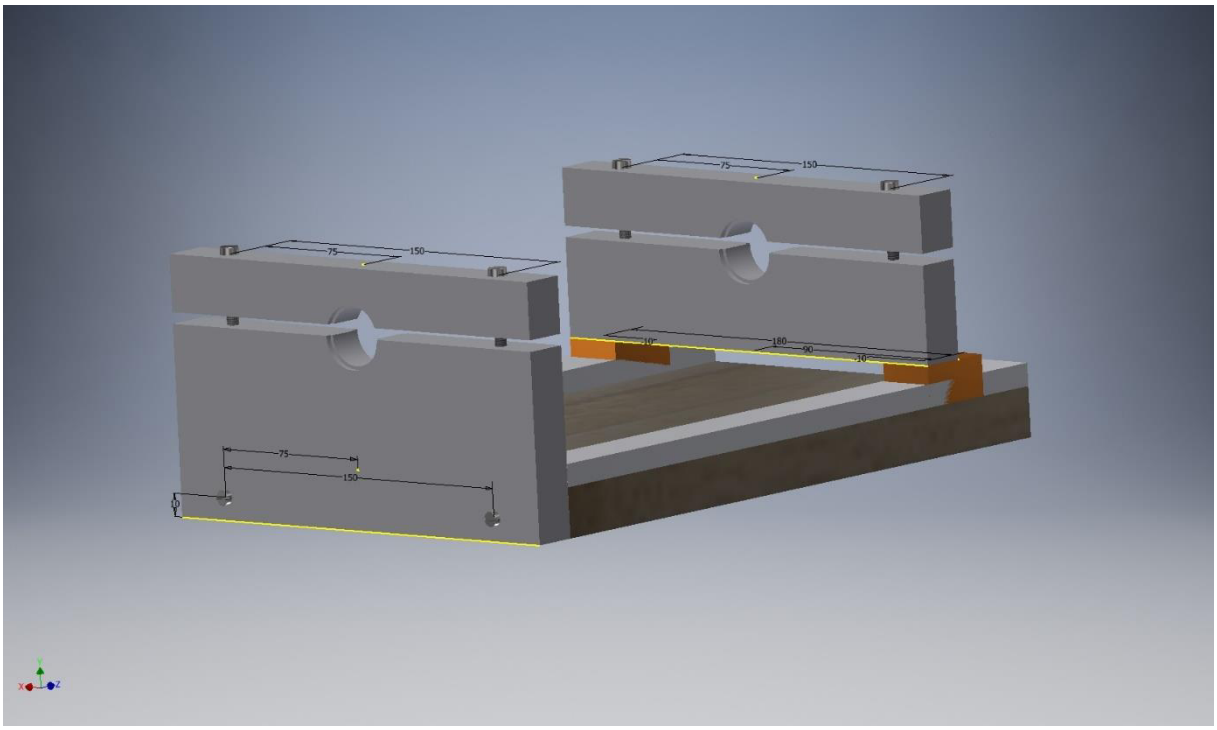

Figure 30: 3D view of the constructed bracket

In the following pages, the technical drawings are attached.

B-B (1 : 2)

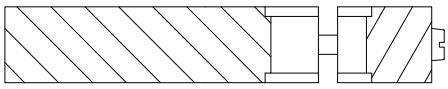

A-A (1 : 2)

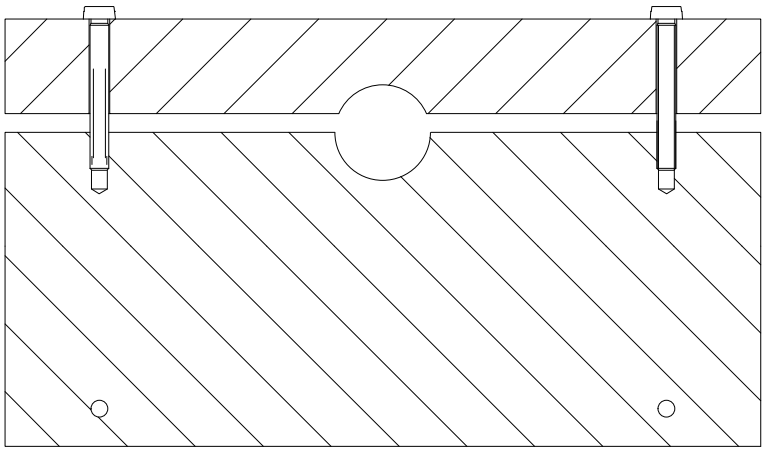

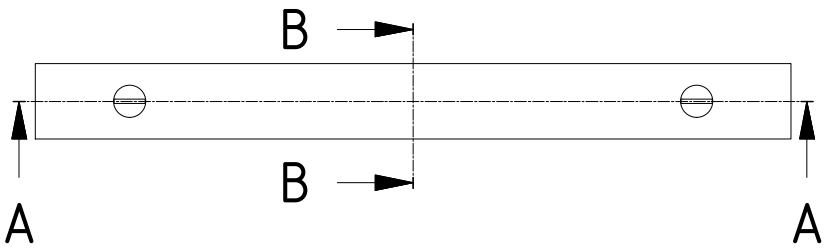

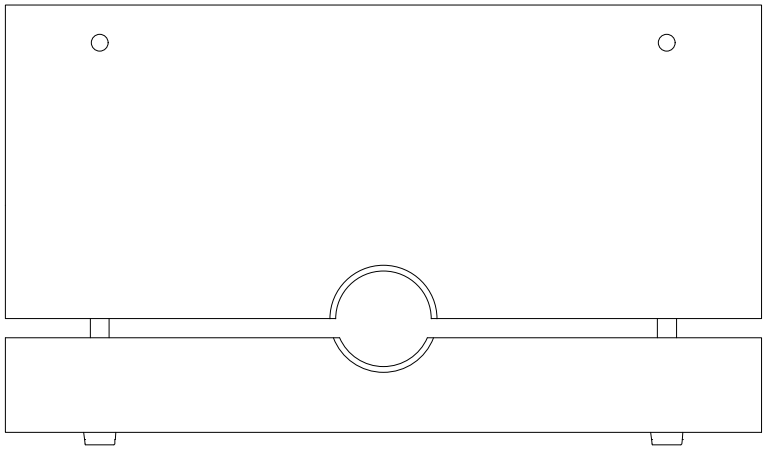

					Datum	Name
				Gezeichnet		K. Randhawa
				Kontrolliert		
				Norm		

Fix Bracket

					1
					A4
Status	Änderungen	Datum	Name		

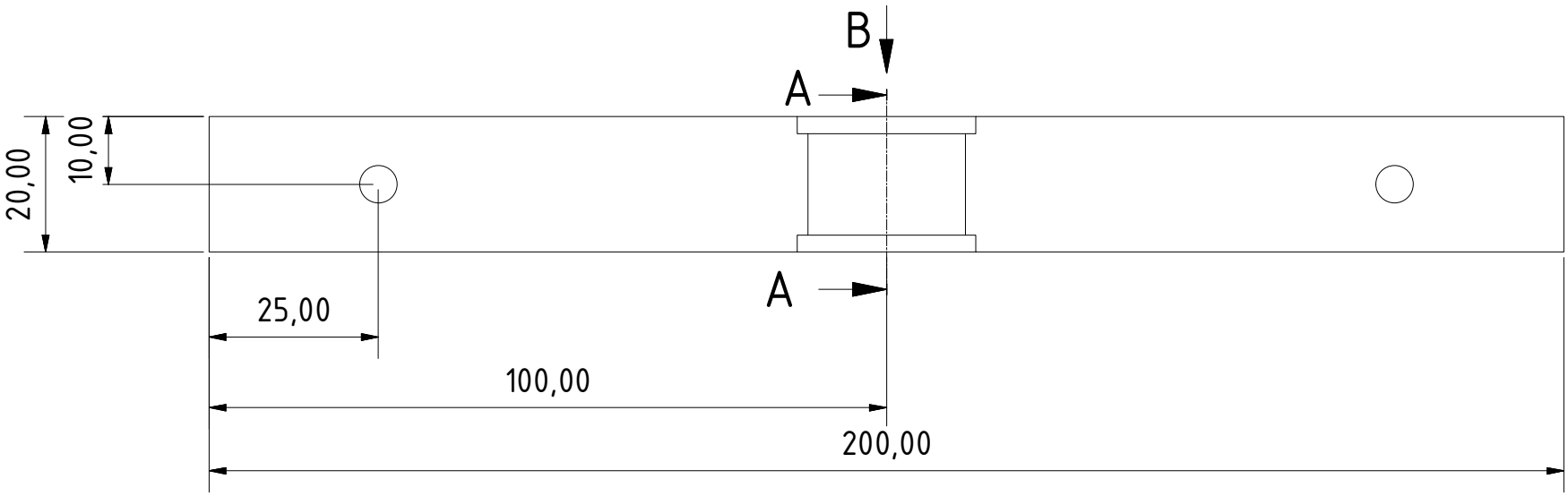

B (1 : 1)

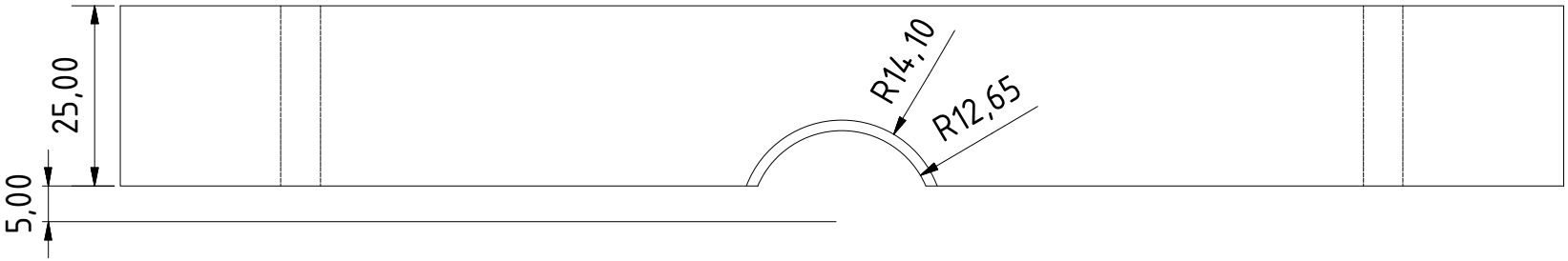

A–A (1 : 1)

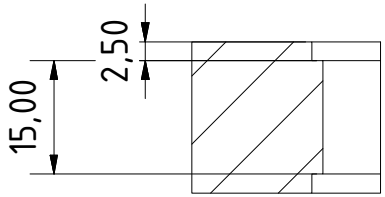

					Datum	Name
				Gezeichnet		csr4162
				Kontrolliert		
				Norm		
Status	Änderungen	Datum	Name			

Head of the Bracket

1

A4

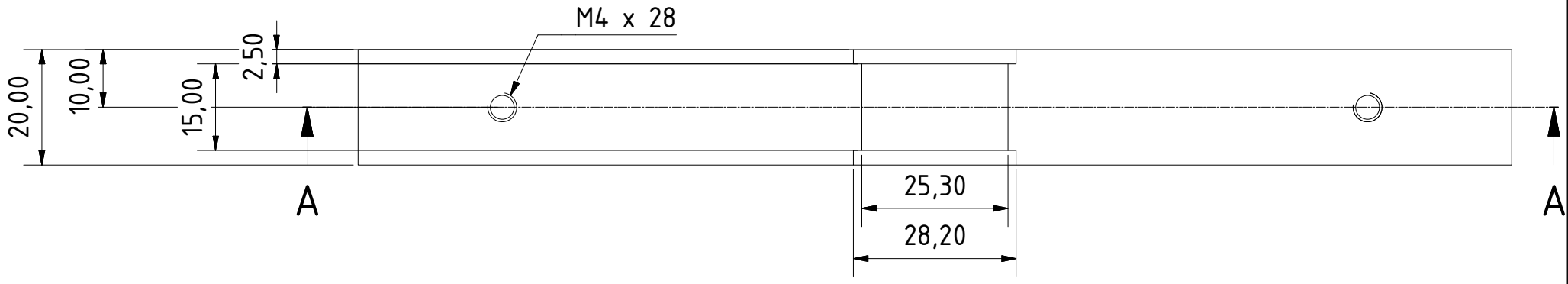

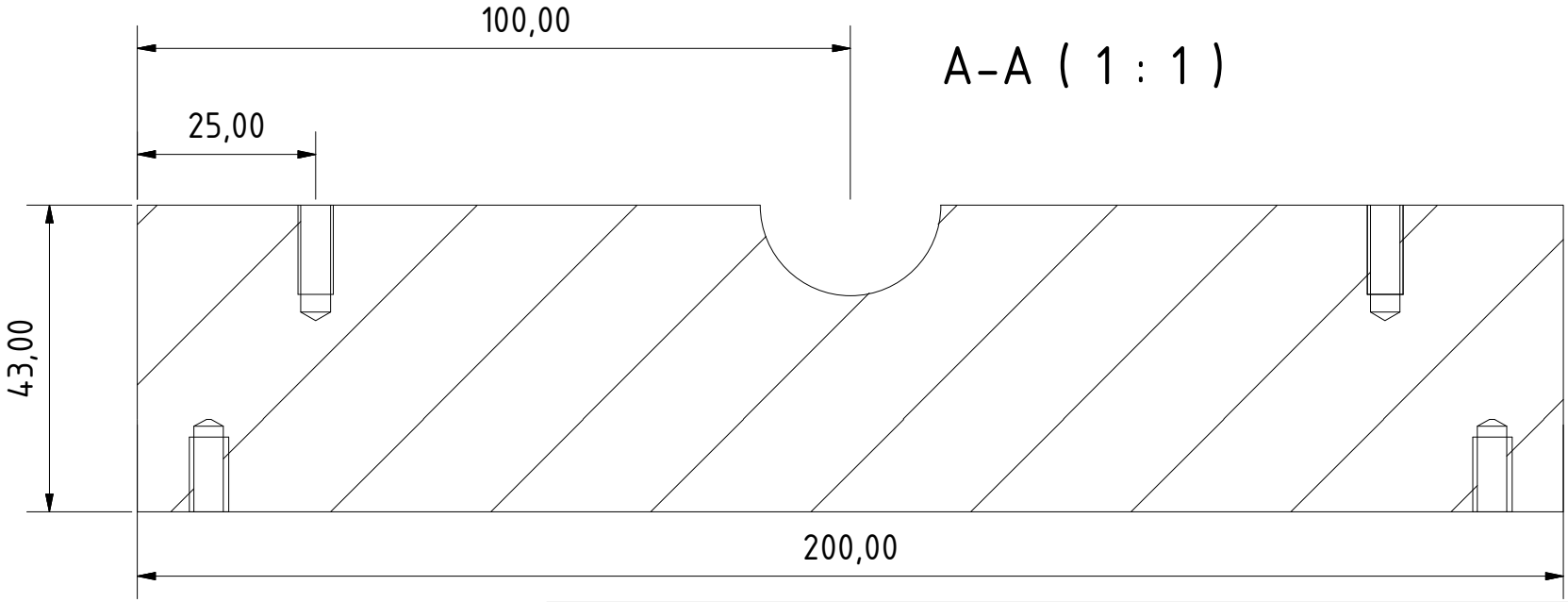

A–A (1 : 1)

					Datum	Name
				Gezeichnet		csr4162
				Kontrolliert		
				Norm		
Status	Änderungen	Datum	Name			

Flexible Bracket - Body

1

A4

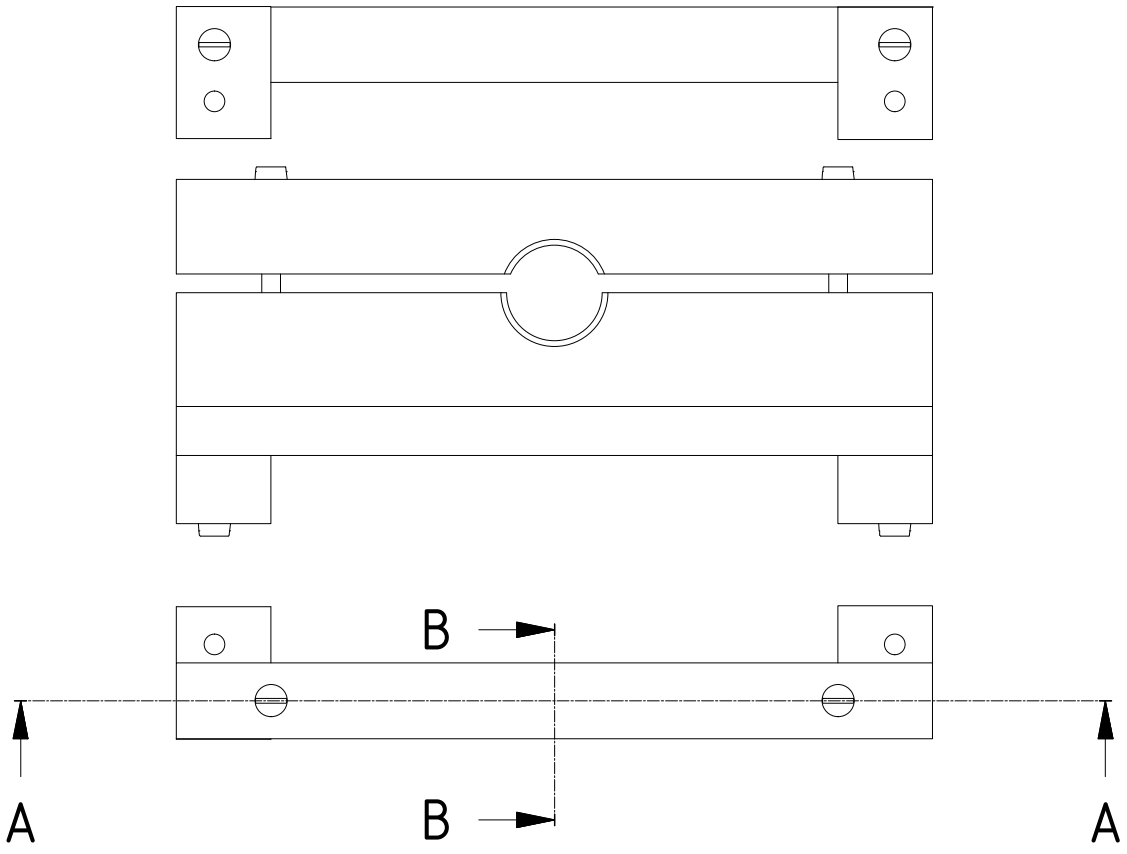

B-B (1 : 2)

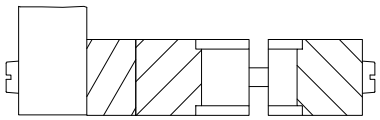

A-A (1 : 2)

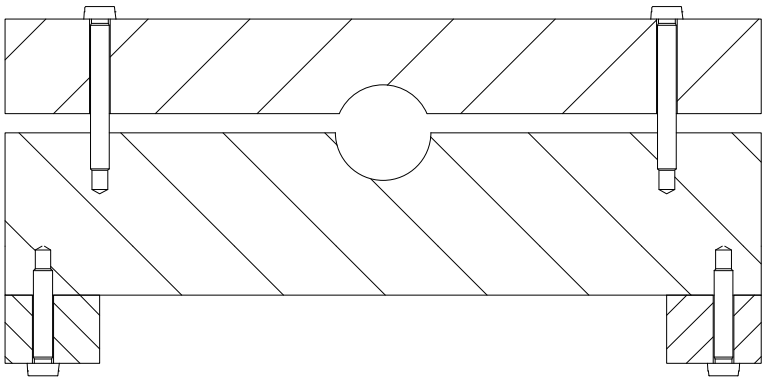

					Datum	Name
				Gezeichnet		csr4162
				Kontrolliert		
				Norm		
Status	Änderungen	Datum	Name			

Flexible Bracket

1

A4

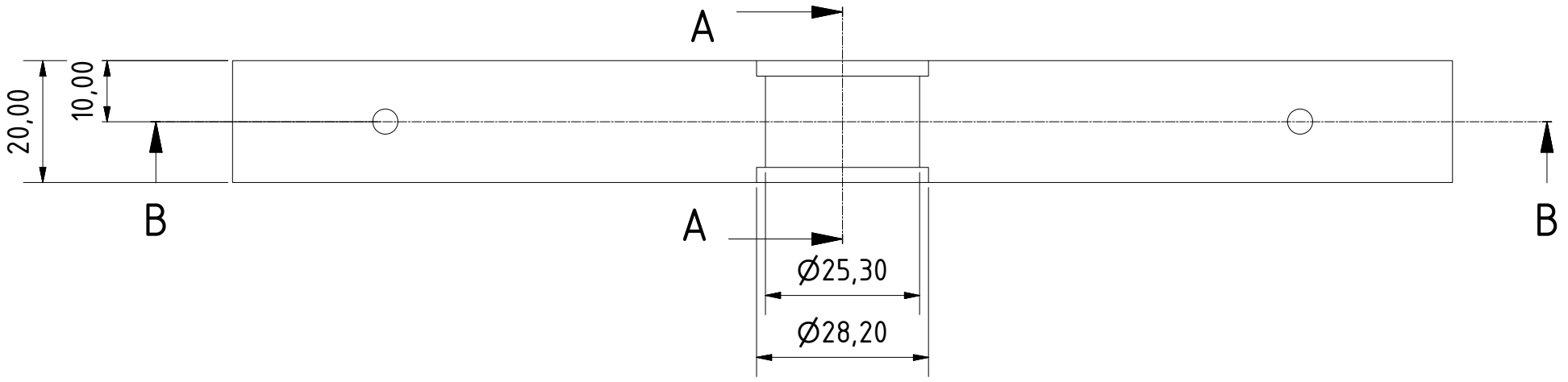

A-A (1 : 1)

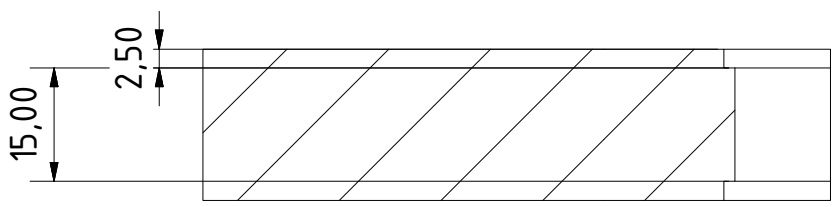

B-B (1 : 1)

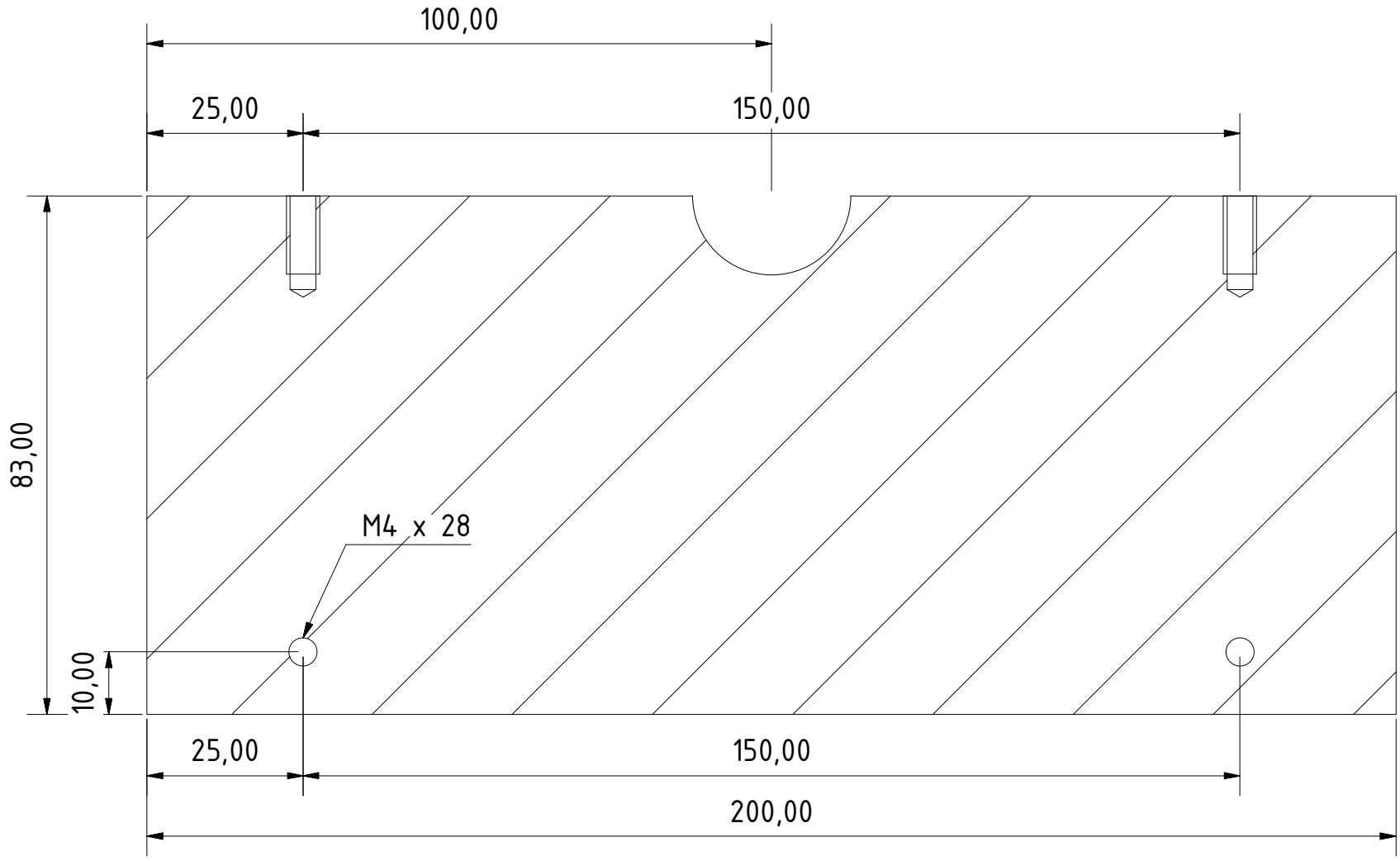

					Datum	Name
				Gezeichnet		csr4162
				Kontrolliert		
				Norm		
Status	Änderungen	Datum	Name			

Fix Bracket - Body

1

A3